공학석사학위논문

Fouling Resistant Microfiltration (MF) Membrane Modified with Thermo-Reversible Magnetite Nanoparticles

열가역성 자성입자로 개질된 내오염성 정밀여과 분리막의 연구

2017 년 2 월

서울대학교 대학원

재료공학부

우 승 택

Fouling Resistant Microfiltration (MF) Membrane Modified with Thermo-Reversible Magnetite Nanoparticles

열가역성 자성입자로 개질된 내오염성 정밀여과 분리막의 연구

지도교수 곽 승 엽

이 논문을 공학석사 학위논문으로 제출함

2017 년 1 월

서울대학교 대학원

재료공학부

우 승 택

우 승 택의 공학석사 학위논문을 인준함

2017 년 1 월

위 원 장 _____ (인)

부위원장 _____ (인)

위 원 _____ (인)

ABSTRACT

Fouling Resistant Microfiltration (MF) Membrane Modified with Thermo-Reversible Magnetite nanoparticles

Seungtaek Woo

Department of Materials Science and Engineering

The Graduate School

Seoul National University

We developed a dual stimuli-responsive Poly(tetrafluoroethylene) (PTFE) microfiltration (MF) membrane by thermo-responsive covalent attachment of magnetite nanoparticles. Magnetite-modified PTFE membrane had an excellent anti-fouling performance by magneto-rotation induced vortex as well as enhanced cleaning efficiency. To achieve this, a dynamic covalent bonding that responds to the change of temperature called as Diels-Alder cycloaddition, was introduced. Maleimide-terminated magnetite

nanoparticles were synthesized by co-precipitation method of two precursors and polyethylene glycol methyl ether maleimide (PEG-Mal). Various concentration of PEG-Mal was tested to measure the optimized amount of PEG-Mal. A common PTFE MF membrane with the average pore diameter of 0.1 μm was modified with furan functionality by surface UV treatment under hydrazine vapor followed by addition of furfuryl glycidyl ether. Furan-modified PTFE membrane and maleimide-terminated magnetite nanoparticles were coupled by heat treatment. Successful synthesis of maleimide-terminated magnetite nanoparticles was observed by various characterization methods such as Fourier transform infrared spectroscopy (FT-IR), X-ray diffractometry (XRD), thermogravimetric analysis (TGA) and vibrating sample magnetometry (VSM). Also, X-ray photoelectron spectroscopy (XPS), field emission scanning electron microscopy (FE-SEM) and contact angle measurement were additionally used to define characteristics of magnetite-coupled PTFE membrane. Especially, movement of magnetite nanoparticles by rotating external magnetic field was observed by particle image velocimetry (PIV). Finally, water filtration with deionized (DI) water and foulant solution was conducted to evaluate the performance of magnetite-coupled membrane. The modified membrane shown slow decrease of flux in spite of existence of foulant in the feed solution. Also,

backwashing efficiency was remarkably enhanced from 44.6% to 80.9%, compared to neat-PTFE membrane. Contamination of membrane surface could be easily recovered by replacement of maleimide-terminated magnetite nanoparticles to new one. Declined water flux was restored to 80% of initial flux after regeneration of magnetite nanoparticles. This combination of magneto-induced foulant rejection and renewable surface can make synergetic effect of anti-fouling performance. This membrane can be efficiently applied to submerged membrane filtration system using feed solution with various type of foulants and thick concentration.

Keywords

Microfiltration, Fouling, Membrane, Diels-Alder cycloaddition, Thermo-reversible, poly(tetrafluoroethylene), Magnetite, Nanoparticle

***Student Number*: 2015-20845**

Table of Contents

1. Introduction

Over the past several decades, lack of clean water became more and more serious problem for all over the world. Especially in developing country, millions of people die annually because of diseases induced from unsafe water [1]. Scientists keep made every endeavor to secure enough amount of safe and clean water using techniques such as distillation [2], chemical treatment [3], adsorption [4] and membrane filtration [5]. Among the several water purification techniques, membrane filtration has several advantages such as low energy consumption, time-efficiency and small footprint. Because of these reasons, membrane filtration is regarded as an eco-friendly water purification technology.

Despite the several advantages of membrane purification, however, there is a critical drawback in membrane purification called as fouling. Fouling means the flux inhibition by clogging of membrane. As membrane filtration operating, pollutant in feed water called as foulant adsorbed at the surface of membrane. The adsorbed foulants formed a cake layer and block the passage of pure water. Once fouling occurs, there are some critical problems in membrane such as decrease of durability, additional need of

operating energy and necessity of cleaning. All these factors make the increase of operating cost. Therefore, membrane fouling is a major problem of membrane filtration technology [6].

To solve membrane fouling problem, many approaches were attempted. One of the typical solution is introduction of hydrophilic membrane surface [7]. Most of the foulants are hydrophobic so that cannot be adsorbed to hydrophilic surface. Also, hydrophilic nature of membrane can assist the passage of water through membrane pore. However, introduction of hydrophilic polymer is not perfect solution of membrane fouling problem because it offers insufficient anti-fouling performance. Therefore, hydrophilic surface is combined with other anti-fouling methods. Another approach is introduction of biocidal materials [8] such as silver nanoparticle [9], graphene oxide [10], photocatalyst [11], etc. Organic foulants in membrane surface are killed by these biocidal materials so that biofouling could not occur. This approach is very efficient way for prevention of biofouling, but cannot affect the inorganic foulants such as silica and colloidal clay. A new approach of anti-fouling solution is introduction of stimuli-responsive material at the membrane.

Stimuli-responsive material means material that is capable of

conformational and chemical changes on receiving an external stimulus [12]. Stimuli-responsive materials are classified by sort of external stimuli such as thermo-responsive [13], ion-responsive [14], magneto-responsive [15], pH-responsive [16], etc. These stimuli-responsive materials are widely applied in various kinds of technical field such as drug delivery [17, 18], functional film [19], dye release [20], microscopy [21], hydrogel [22], shape memory composite [23], microfluidic device [24], sonoporation [25] and membrane filtration [26, 27, 28, 29, 30]. This stimuli-responsive membrane have not only an excellent anti-fouling performance, but general influence of all kinds of foulants. Due to these advantages, stimuli-responsive membrane were considered as a novel-water purification technology of next generation [31, 32]. Typical examples of stimuli-responsive membrane are as follows: intensified cleaning of fouled layer using thermo-responsive polymer [33], dynamic polymer brush for foulant rejection [34] and magnetically activated micromixer [35]. Compared to other stimuli-responsive membranes, introduction of magneto-responsive material has advantages such as low energy consumption, easy control of external stimuli and instant effect. Additionally, introduction of fouling-resistant magnetite nanoparticles is a preventive way of fouling because they basically inhibit the adsorption of foulant. Also, price of magnetite is very reasonable compared to other

stimuli-responsive materials according to **Table 1**. Anti-fouling mechanism of the magnetically activated micromixer is rejection of foulant using rotating magnetite nanoparticles. From the surface of membrane, hydrophilic poly(2-hydroxyethyl methacrylate) (PHEMA) chain is introduced using atom transfer radical polymerization (ATRP) technique and terminated with magnetite nanoparticles. When membrane filtration is in operation, external rotating magnetic field is applied and this magnetite nanoparticles are rotating in the water. The movement of magnetite nanoparticles induces the magneto-induced vortex of water and foulants are physically rejected from the membrane surface. This method can not only prevent membrane fouling, but also reduce concentration polarization. Also, magneto-responsive anti-fouling membrane is efficient to all kinds of foulants because of its physical mechanism of anti-fouling. This magneto-responsive anti-fouling membrane, however, has poor cleaning efficiency. In conclusion, magneto-responsive membrane is effective anti-fouling membrane, but enhancement of cleaning efficiency is required.

Here, we prepared an advanced magneto-responsive membrane with renewable magnetite nanoparticles on the surface using thermo-responsive dynamic covalent bonding of furan and maleimide. This furan-maleimide

bonding is called Diels-Alder cycloaddition [36] which is reversibly formed and deformed by change of temperature. Maleimide-terminated magnetite nanoparticles were synthesized by simple co-precipitation method. Also, conventional PTFE membrane was modified with furan functionality by UV treatment. This furan-modified PTFE membrane and maleimide-terminated magnetite nanoparticles were coupled each other using Diels-Alder cycloaddition. Physical and chemical properties of maleimide-terminated magnetite and magnetite-coupled PTFE membrane were identified by various characterization methods. Especially, the generation of magneto-induced vortex was identified by particle image velocimetry (PIV). The performance of membrane was tested by water filtration test with Lysozyme and silica colloidal solution. Also, irreversible fouling due to the continuous operation of membrane filtration was resolved by regeneration of magnetite nanoparticles.

Peel-and-stick process of magnetite nanoparticles can reproduce the anti-fouling characteristics of membrane without whole replacement of membrane itself. PTFE membrane is quite expensive membrane so this reuse of PTFE membrane has an economical advantage rather than replacement with new one. Additionally, synthesis of existing magneto-responsive

membrane is not easy because synthesis condition of it is quite harsh. Renewable magneto-responsive PTFE membrane, however, can be synthesized by simple coupling of pre-synthesized maleimide-terminated magnetite nanoparticles and modified PTFE membrane. Therefore, mass production of membrane is much simple using dynamic covalent bonding. This fouling-resistant membrane using multiple anti-fouling methods has excellent anti-fouling performance because of synergetic effect. This outstanding fouling resistance can be valuable in membrane filtration system under harsh fouling condition such as thick foulant concentration complexed composition of foulants, such as submerged membrane system.

	Price(KRW) Ref : Sigma-Aldrich	Control method	Purpose
Thermo-responsive (NIPAM)	**12400 / g**	**Temperature rising** (High energy consumption, slow speed of heating)	**Washing**
Ion-responsive (SVBP)	**8810 / g**	**Addition of NaCl** (NaCl itself works as impurity)	**Washing**
Magneto-responsive (Magnetite)	**1644 / g**	**Magnetic field control** (Low energy consumption, Instant effect)	**Prevention of fouling**

Table 1. Comparative description of stimuli-responsive materials

2. Experimental section

2.1. Materials

A porous poly(tetrafluoroethylene) (PTFE) flat sheet membrane with 47 mm diameter and 0.1 μm average pore size was purchased from Advantec-MFS, INC. (Tokyo, Japan). Iron chloride(II) tetrahydrate(97%), Iron chloride(III) hexahydrate(97%), Poly(ethylene glycol) methyl ether maleimide (PEG-Mal) (M_n 2000), Furfuryl glycidyl ether (96%), hydrazine monohydrate (98%), Lysozyme for chicken egg white, and LUDOX SM-30 (30 wt% silica suspension, average particle size was 7 nm) was purchased from Sigma-Aldrich (St Louis MO, USA). Toluene (99.8%), tetrahydrofuran (THF, 99.0%) were purchased from Daejung Chemical & Metals (Gyeonggi-do, Korea). The aqueous solutions were prepared with deionized (DI) water.

2.2. Synthesis of Maleimide-terminated magnetite (MG@PEG-Mal)

Synthesis of magnetite nanoparticle by co-precipitation method and modification of magnetite nanoparticle with PEG-Mal were done simultaneously. 290 mg of Iron chloride(II) tetrahydrate, 720 mg of Iron chloride (III) hexahydrate and PEG-Mal were put into 50 ml 3-neck round flask and 5 ml of DI water was added. The amount of PEG-Mal was varied from 0.5 g to 3 g. The orange-colored solution was stirred with magnetic stirrer and sealed followed by N_2 gas purging. After that, 5ml of 25 wt% NH_4OH aqueous solution was slowly added by dropping funnel for 10 minutes. Black colored magnetite was rapidly precipitated from orange-colored solution and the suspension solution was stirred continuously for 3 hours. After then, magnetite nanoparticle was separated by magnetic decanting using neodymium-boron permanent magnet and washed with DI water and Ethanol to remove unreacted precursors and residues. Every washing process was done with 30 minutes of ultrasonic wave treatment for clean washing of interparticle residues. Final product was suspended into THF. Overall scheme is subscribed in **Figure 1**.

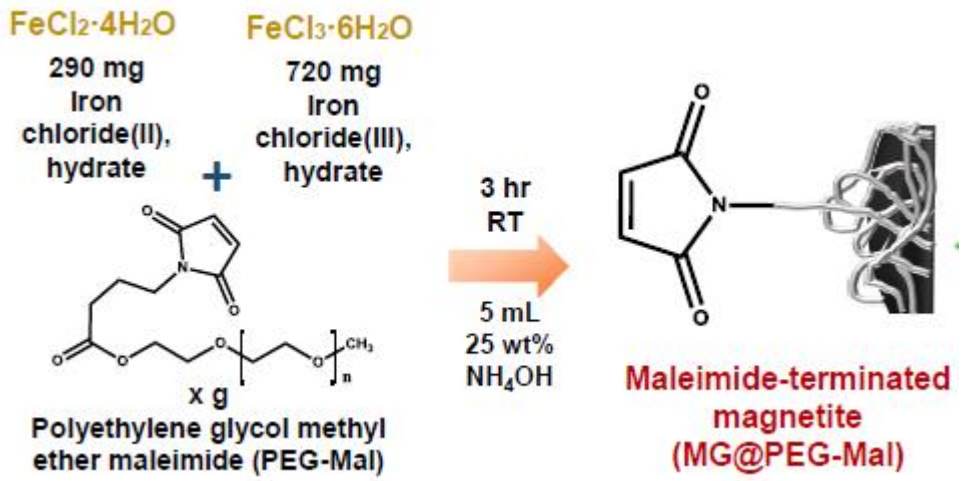

Figure 1. Schematic illustration of synthesis of MG@PEG-Mal

2.3. Fabrication of furan-modified PTFE membrane

20 ml of hydrazine monohydrate was put into 50 ml beaker and 15 g of sodium hydroxide bead was added to obtain dehydrated hydrazine. 3 sheets of PTFE flat sheet membrane and dehydrated hydrazine were placed into quartz cell and filled with N_2 gas. The PTFE membrane was exposed to UV light irradiation (λ_{max} = 254 nm, 100 W) for 72 hours. After the reaction, the surface-aminated PTFE membrane was washed with THF and dried under vacuum oven overnight. Next, 1.4 ml of Furfuryl glycidyl ether was added on both side of surface-aminated PTFE membrane. The membrane was placed in 50 ˚C oven overnight. The furan-modified PTFE membrane was rinsed with THF, Ethanol and DI water for several times for removal of unreacted chemicals and dried under vacuum oven overnight. All the steps of membrane modification was illustrated at **Figure 2**.

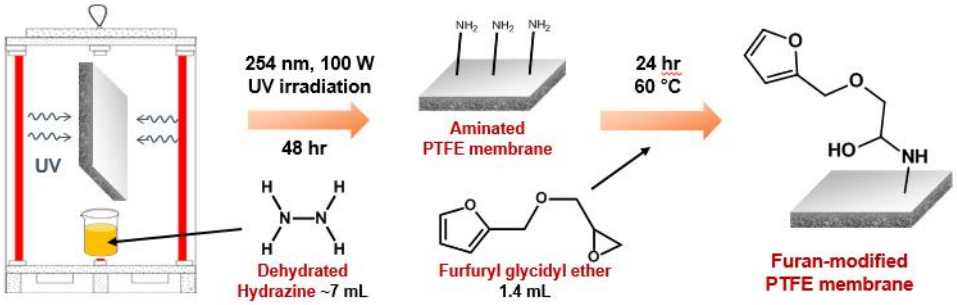

Figure 2. Schematic illustration of fabrication of furan-modified PTFE membrane

2.4. Fabrication of magnetite-coupled PTFE membrane (MG-PTFE)

Furan-modified PTFE membrane was placed on petri dish and wetted with 1 ml of THF. On both side of wetted furan-modified PTFE membrane, 1.4 ml of magnetite nanoparticle-THF suspension solution was and placed in 50 ˚C shaking oven for 24 hours. After the Diels-Alder reaction, the membrane was rinsed with THF, Ethanol and DI water to remove unreacted chemicals and treated with ultrasonic wave to remove loosely attached magnetite nanoparticles. The final product was dried under vacuum oven overnight. Magnetite coupling using Diels-Alder cycloaddition of furan and maleimide functionalities was described at **Figure 3**.

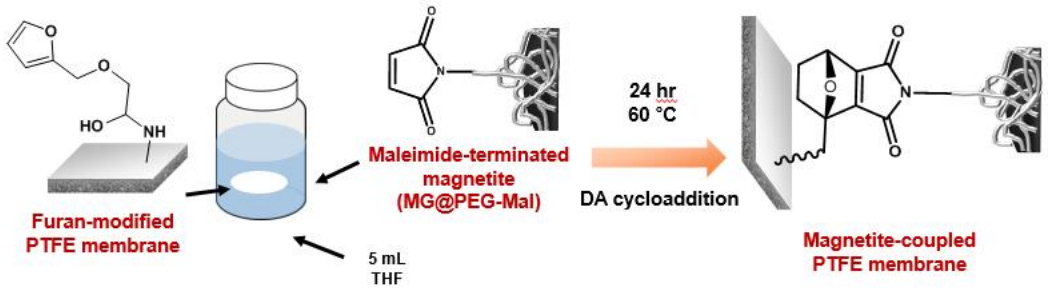

Figure 3. Schematic illustration of fabrication of MG-PTFE membrane

2.5. Peel-and-stick process of MG@PEG-Mal

The MG@PEG-Mal layer can be freely removed and re-attached by thermo-responsive dynamic covalent bonding. As previously described, Diels-Alder cycloaddition under 50 ˚C can be used for attachment of MG@PEG-Mal on the PTFE membrane. To remove MG@PEG-Mal from the surface of furan-modified PTFE membrane, retro Diels-Alder (rDA) cycloaddition was used. MG-PTFE membrane was immersed in 100 ml toluene and the solution was heated under 150 ˚C for 24 hours with reflux. After the rDA reaction, the membrane was rinsed with THF, Ethanol and DI water with ultrasonic wave treatment to remove loosely attached magnetite nanoparticles. The rinsed furan-modified PTFE membranes were dried under vacuum oven overnight. Also, the peeled magnetite nanoparticles were collected by magnetic decanting and dried to evaluate durability of PEG-Mal layer on the surface of magnetite nanoparticles.

2.6. Characterization

Chemical structure of synthesized MG@PEG-Mal was monitored by Fourier transform infrared (FT-IR, Thermo Scientific Nicolet iS1) spectroscopy with a spectral resolution of 4 cm^{-1} with the range of 500-4000 cm^{-1}. Crystal structure of magnetite samples were observed by X-ray diffractometer (XRD, New D8 Advance) with 2theta range of 20-80 degree and 0.154 nm of wavelength. Mass of introduced PEG-Mal polymer on the surface of magnetite nanoparticle was measured by thermogravimetric analysis (TGA, Q-5000IR) with temperature range of 25-600 °C. Magnetization of MG@PEG-Mal was measured by vibrating sample magnetometer (VSM, EV9-380V) system.

Neat, aminated, furan-modified and magnetite-coupled PTFE membrane were characterized by attenuated total reflection Fourier-transform infrared (ATR FT-IR, Thermo Scientific Nicolet iS5) spectroscopy with a spectral resolution of 4 cm^{-1} with the range of 650-4000 cm^{-1} and X-ray photoelectron spectroscopy (XPS, Kratos AXIS-His) using monochromatic Mg Kα X-ray source operated at 10 mA. The surface morphology of membranes were observed by field-emission scanning electron microscope (FE-SEM, SUPRA 55VP) with surface platinum coating

and energy dispersive spectroscopy (EDS). To evaluate change of the membrane surface hydrophilicity, static pure water contact angle measurement (Biolinscientific, Attention® THETA LITE) was used under room temperature. The external magnetic field was applied using rotating neodymium-boron permanent magnet connected to mechanical stirrer (Wisestir® HT50AX). Finally, the motion of magnetite nanoparticle in the water responding to external rotating magnetic field was directly observed by particle image velocimetry (PIV, MGL10000) observation with exposure time of 11000 μs and 0.135 μm of pixel size. Schematic explanation of PIV observation is shown at **Figure 4**. Silica nanoparticle with average diameter of 10 μm was dispersed to the pure water and monochromatic green laser with 527 nm of wavelength was projected perpendicular to camera lens for inducing scattering of silica nanoparticle. The result was analyzed by cross-correlation method using formula as follows:

$$(f*g)(\tau)\stackrel{\text{def}}{=}\int_{-\infty}^{\infty} f^*(t)g(t+\tau)dt$$

where f and g are continuous function, f* is the complex conjugate of f and τ is the lag of time.

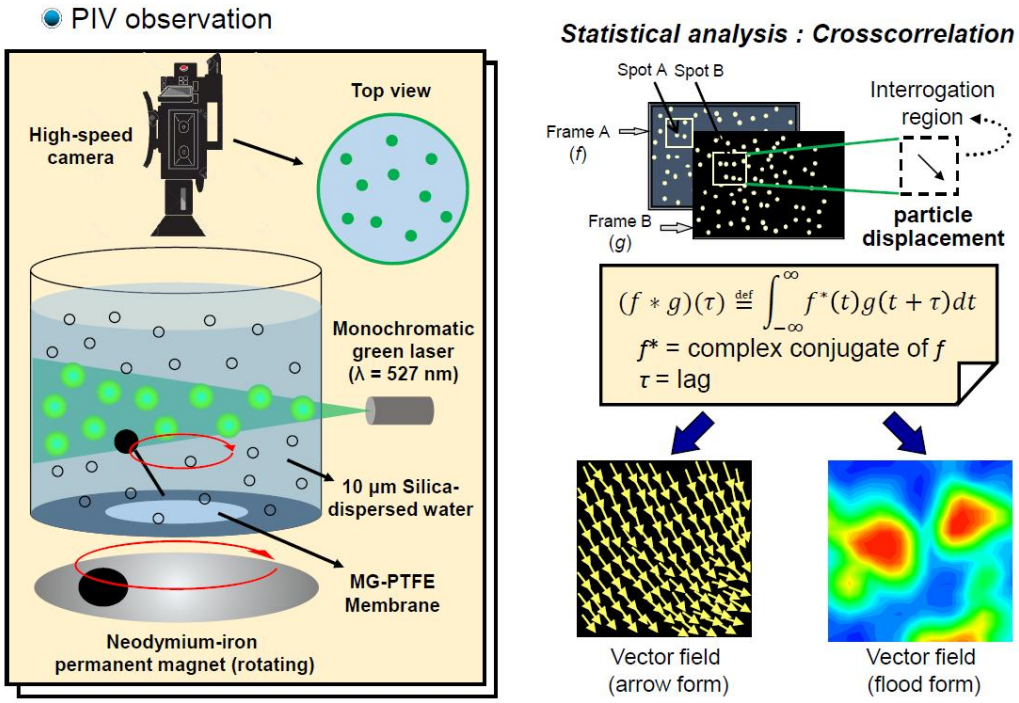

Figure 4. Schematic illustration of PIV observation

2.7. Evaluation of fouling resistance

Anti-fouling property of neat, aminated, furan-modified and MG-PTFE membrane was measured by pure water filtration system. To investigate anti-biofouling property, 500 ppm Lysozyme solution consisted of 500 mg of Lysozyme from chicken egg white and 1L of pure water was used. Next, anti-inorganic fouling behavior was measured by filtration using 500 ppm LUDOX SM-30 solution. All the chemicals were used without further purification.

Water filtration was performed using Amicon® 8010 dead-end stirred cell (Millipore Corp.) connected with pressure vessel filled with pure water or foulant solution. The filtration system was described at **Figure 5**. The operating pressure was 0.2 bar. Before starting the filtration, all membranes were wetted with ethanol and experienced 30 minutes of pure water filtration under 0.2 bar of pressure. After per times of fouling test, 10 minutes of backwashing at 0.2 bar was done to remove loosely attached foulants from membrane surface. Water flux was calculated by collecting permeate and measuring mass using analytic mass balance (CAS CUW 420H) and using the equation as follows:

$$\text{Flux} = Q/(t * A)$$

where Q is the volume of the permeate (L), t is the filtration time (hours) and A is the effective area of the membrane (m^2). Cleaning efficiency of membrane by backwashing or peel-and-stick process was measured by calculating flux recovery ratio (FRR), which is indicated according to the formula as follows:

$$\text{FRR} = \frac{J_R}{J_0} \times 100$$

Where J_R is the water flux of cleaned membrane and J_0 is the initial water flux. Finally, the degree of membrane fouling was represented by calculated reversible and irreversible fouling resistance:

$$R_r = \frac{J_R - J_P}{J_0} \times 100$$

$$R_{ir} = \frac{J_0 - J_R}{J_0} \times 100$$

Where R_r and R_{ir} are the reversible and irreversible fouling resistance, respectively and J_p is the flux of foulant solution.

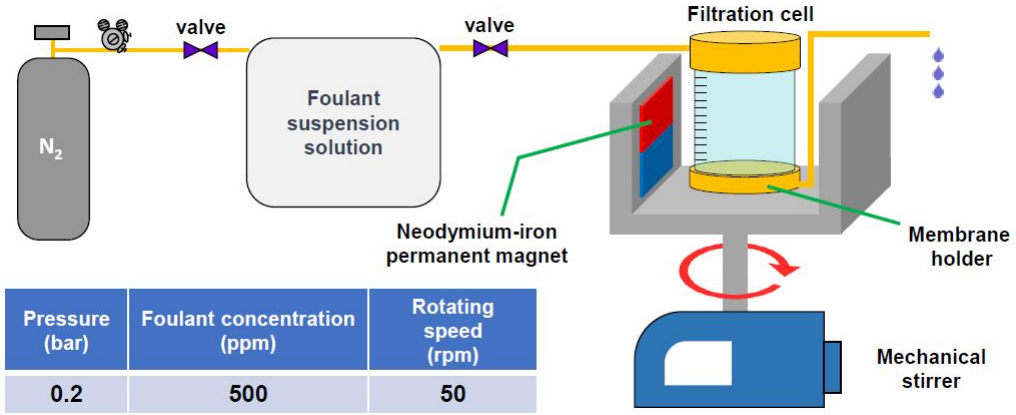

Pressure (bar)	Foulant concentration (ppm)	Rotating speed (rpm)
0.2	500	50

Figure 5. Schematic description of water filtration system

3. Results and discussion

3.1. Synthesis of MG@PEG-Mal

Due to the screening effect of PEG-Mal polymer on the surface of magnetite, certain degree of magnetization loss is inevitable. Meanwhile, enough amount of maleimide functionality is necessary for stable bonding of maleimide functionality of MG@PEG-Mal and furan functionality of furan-modified PTFE membrane. For this reason, there is a trade-off between the strength of covalent bonding and magnetization according to the amount of PEG-Mal polymer. To find the best amount of PEG-Mal, the amount of PEG-Mal was set as variable just like described in **Table 2**.

Chemical structure of MG@PEG-Mal was observed by FT-IR spectra. As shown in **Figure 6**, the characteristic peaks of PEG-Mal is C-H stretch at 2870 cm^{-1}, C-O stretch at 1050 cm^{-1} and C=O stretch at 1705 cm^{-1}. Especially, C=O stretch is the most important and clear evidence of existing maleimide functionality. Also, the characteristic peaks of magnetite are O-H stretch at 3400 cm^{-1} and Fe-O stretch at 650 cm^{-1}. For MG@PEG-Mal 0.5, the sample synthesized with 0.5 g of PEG-Mal polymer, all characteristic peaks of magnetite were observed while no characteristic peaks of PEG-Mal existed. This result indicated that 0.5 g of PEG-Mal was not enough amount

to synthesize PEG-Mal coated magnetite. However, all characteristic peaks of PEG-Mal including C=O stretch were well observed at MG@PEG-Mal 1. All the characteristic peaks of magnetite were also observed in MG@PEG-Mal 1. That is, 1 g of PEG-Mal polymer was enough amount of successfully coat PEG-Mal polymer on the surface of magnetite nanoparticles. MG@PEG-Mal 2 and MG@PEG-Mal 3 had same tendency with MG@PEG-Mal 1. To summarize, magnetite nanoparticle coated with PEG-Mal polymer was successfully synthesized with 1g of PEG-Mal polymer.

Crystal structure of magnetite samples were measured by XRD pattern. As shown in **Figure 7**, the relative magnitude and position of peaks were identical to the reference of JCPDS # 19-0629 (magnetite). Also, the average magnitude of peaks were decreased if PEG-Mal coating was performed. This is because the screening effect of PEG-Mal polymer on the surface of magnetite nanoparticles. This result indicated the successful synthesis of magnetite samples coated with various concentration of PEG-Mal polymer. Additionally, the crystal grain size was calculated according to Scherrer equation described as follows:

$$d = \frac{K\lambda}{\beta \cos\theta}$$

Where d is the crystal grain size of magnetite, K is a dimensionless shape factor with a value typically close to 0.9, λ is the wavelength of X-ray, β is the line broadening at half the maximum intensity (FWHM) after subtracting the instrumental line broadening in radians. The calculated result was arranged in **Table 3**, and all the grain size was similar. To summarize, magnetite samples were successfully synthesized and PEG-Mal coating on the surface of magnetite nanoparticle was indirectly observed.

Coating of PEG-Mal polymer was observed by TGA analysis. As shown in **Figure 8**, the weight loss of PEG-Mal polymer was occurred at the temperature range of 300-400 ˚C. Compared with bare magnetite, MG@PEG-Mal samples were experienced the weight loss at the temperature range of 300-400 ˚C. This result indicated the PEG-Mal coating on the surface of magnetite nanoparticles. The weight loss was described in **Table 4**, by comparing the weight at 25 ◦C and at 600 ˚C and this value means the introduced amount of coated PEG-Mal. To be specific, MG@ PEG-Mal 0.5 had no significant difference with bare magnetite, but there was a drastic increase of introduced PEG-Mal amount if at least 1 g of PEG-Mal was used. For MG@PEG-Mal 2 and MG@PEG-Mal 3, the introduced amount of PEG-Mal was slightly increased, but the degree of increase was not serious. To

summarize the TGA result, at least 1 g of PEG-Mal was necessary to synthesize MG@PEG-Mal, but using too much amount of PEG-Mal was not effective way. Therefore, MG@PEG-Mal 1 was the optimized sample to synthesize MG-PTFE.

The magnetization of magnetite samples were measured by VSM analysis. PEG-Mal modification induced decline of saturation magnetization (Ms) according to **Figure 9**. Compared with bare magnetite, MG@PEG-Mal had less magnetization, but the degree of decline was not serious according to **Table 5**. For these reasons, PEG-Mal was successfully introduced on the magnetite with optimized amount of hydrophilic polymer and without critically hinder the magnetic property of magnetite nanoparticle.

Sample code: MG@PEG-Mal x
MG@PEG-Mal 0.5
MG@PEG-Mal 1
MG@PEG-Mal 2
MG@PEG-Mal 3

Table 2. The amount of PEG-Mal set as an experimental variable

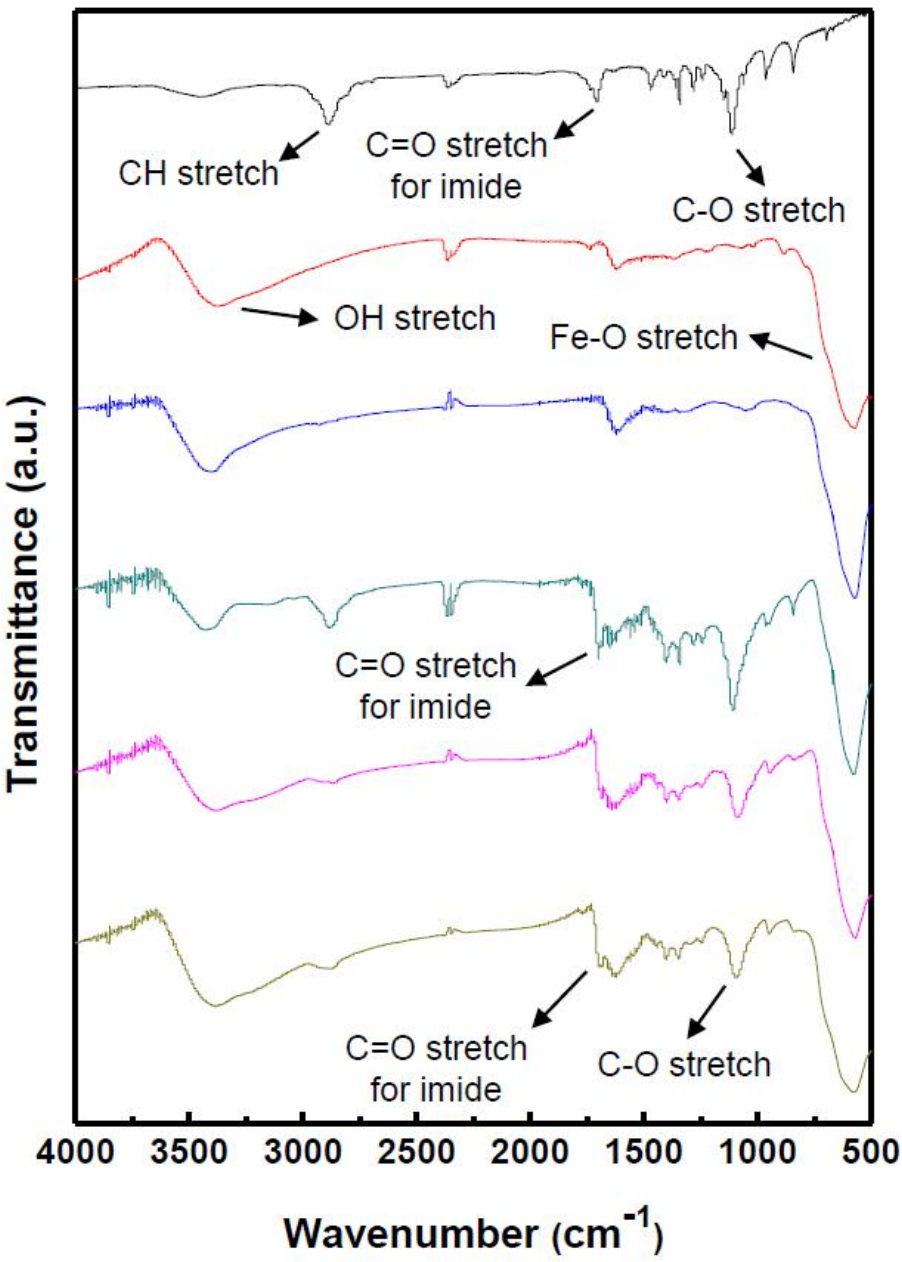

Figure 6. FT-IR spectra of magnetite, PEG-Mal and MG@PEG-Mal samples

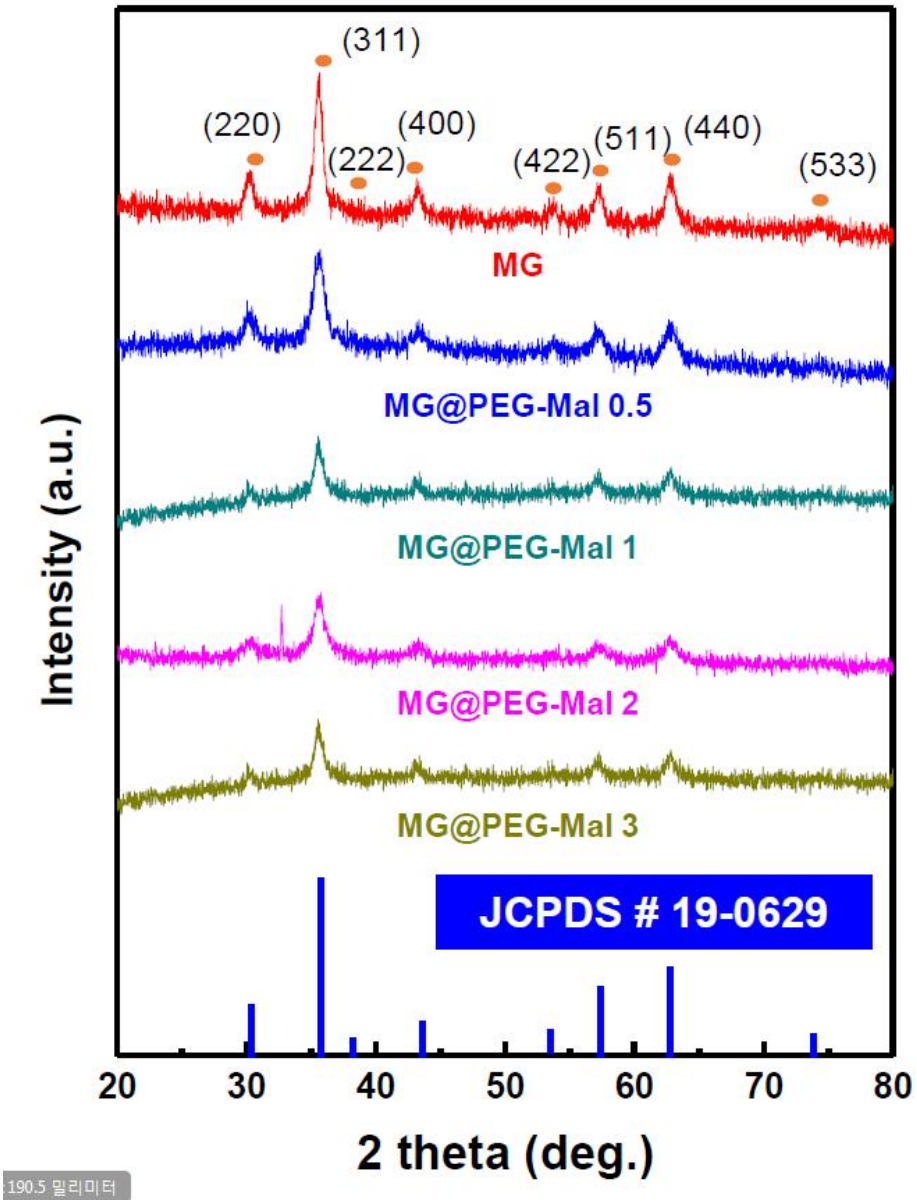

Figure 7. XRD pattern of magnetite samples

	β (rad)	d (nm)
MG	0.0082	17.75
MG@PEG-Mal 0.5	0.0083	17.54
MG@PEG-Mal 1	0.0082	17.75
MG@PEG-Mal 2	0.0081	17.97
MG@PEG-Mal 3	0.0081	17.97

Table 3. Calculated crystal grain sizes of magnetite samples

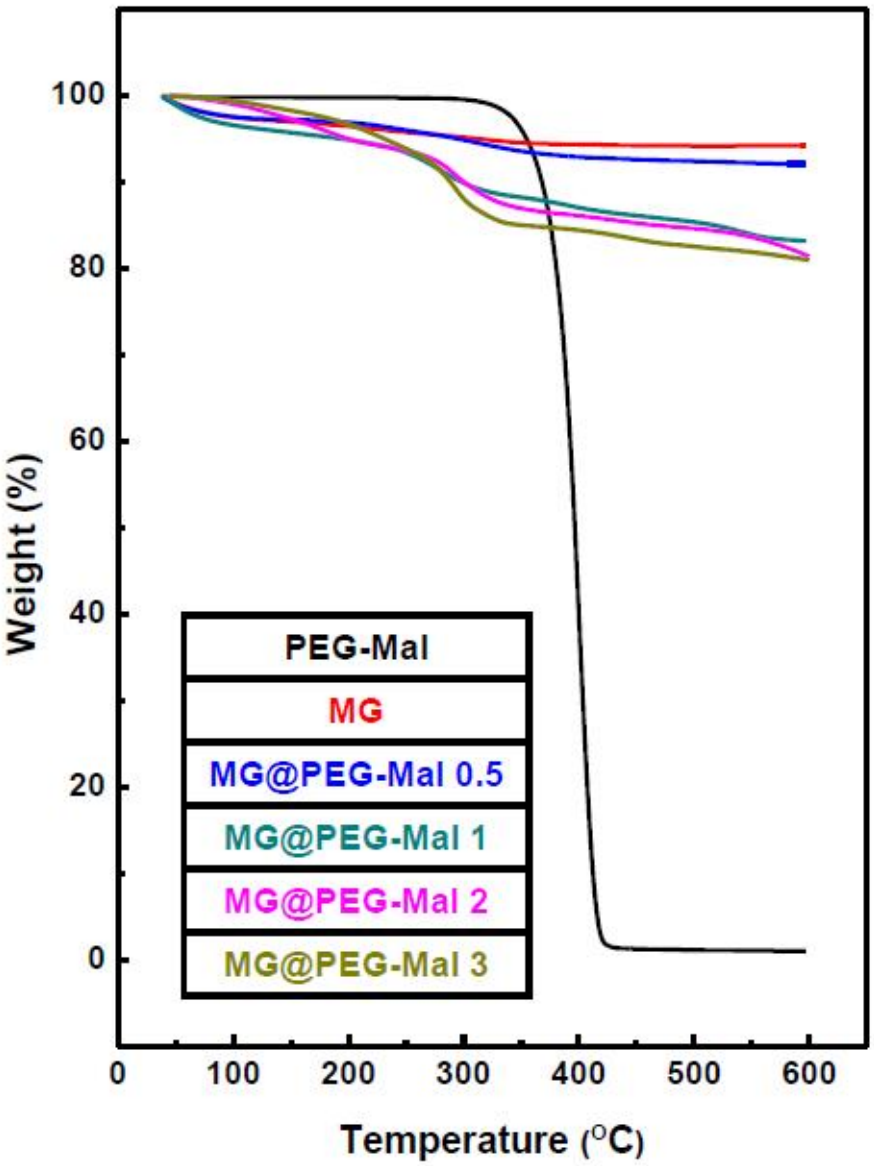

Figure 8. TGA analysis result of PEG-Mal and magnetite samples

Sample	Weight loss (%)
MG	5.74
MG@PEG-Mal 0.5	7.83
MG@PEG-Mal 1	16.79
MG@PEG-Mal 2	18.54
MG@PEG-Mal 3	18.99

Table 4. Weight loss percent of magnetite samples

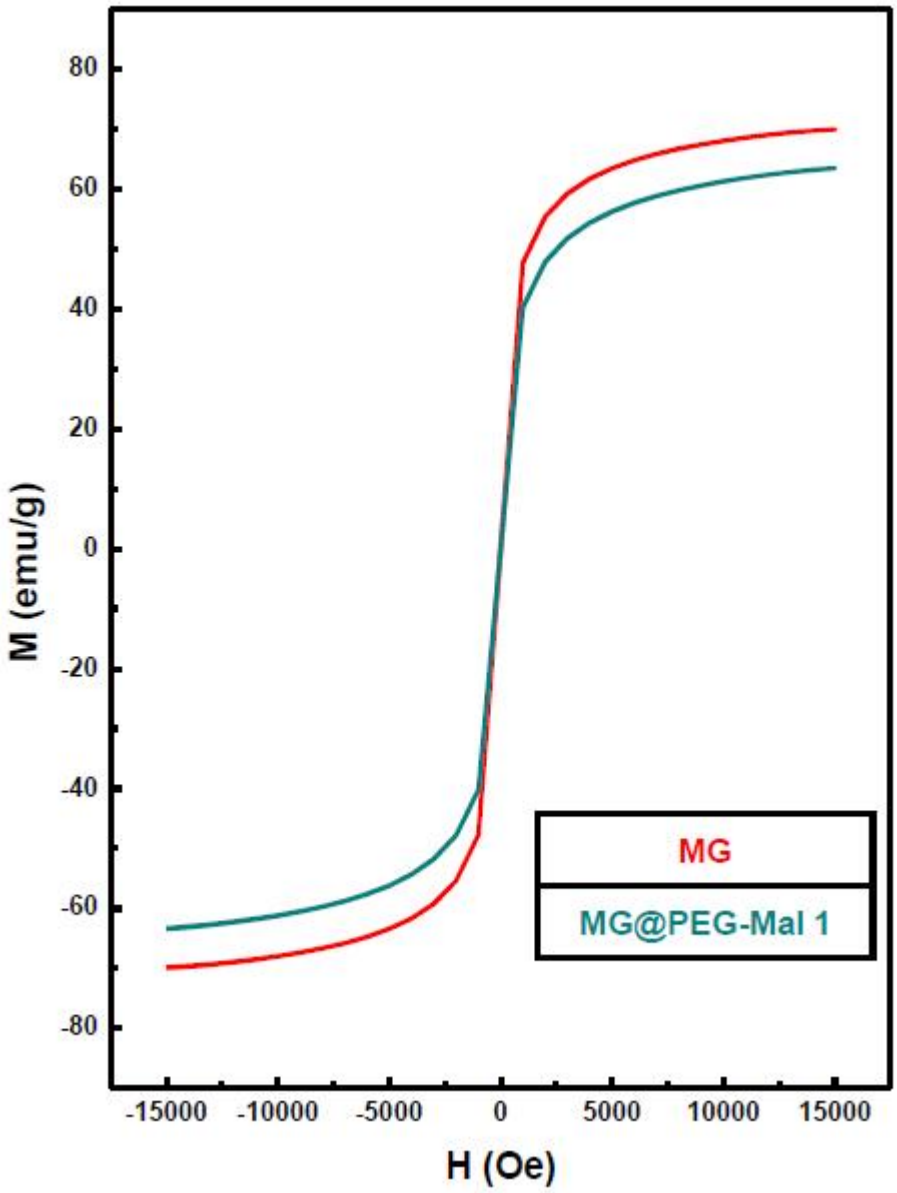

Figure 9. VSM result of magnetite and MG@PEG-Mal 1

Sample	Magnetization (emu/g)
MG	69.90
MG@PEG-Mal 1	63.41

Table 5. Saturation magnetization of two magnetite samples

3.2. Fabrication of MG-PTFE membrane

A conventional PTFE flat sheet membrane was modified with amine functionality by treatment with UV light under hydrazine vapor, and furan functionality was introduced by connecting amine functionality with Furfuryl glycidyl ether. While in these processes, the obvious evidence of introduced amine or furan functionality were the most important factor of successful modification. Also, MG@PEG-Mal was connected with furan functionality by Diels-Alder cycloaddition and magnetite-coupled PTFE membrane was formed. In this process, the new appearance of maleimide functionality or magnetite was the most important evidence of successful synthesis.

The synthesized membrane samples were characterized by ATR FT-IR spectra. **Figure 10** and **Figure 11** shown the overall change of FT-IR peaks of membranes. Compared with neat PTFE membrane, the NH_2 bend at 1619 cm^{-1} newly appeared in aminated PTFE membrane. This indicated the successful amine modification of neat PTFE membrane. Likewise, C=C stretch of furan was observed in furan modified PTFE membrane. The successful furan modification of PTFE membrane could be observed, therefore. Meanwhile, the characteristic peaks of MG@PEG-Mal was OH

stretch at 3400 cm^{-1}, CH stretch at 2800 cm^{-1} and C=O stretch at 1705 cm^{-1}. All these peaks were similarly observed in MG-PTFE sample, but these peaks were not observed in other membranes. These result indicated the successful amination, furan modification and MG@PEG-Mal modification. To summarize, MG-PTFE membrane was successfully synthesized by Diels-Alder cycloaddition.

The modification of membranes were determined by X-ray photoelectron spectroscopy. As seen at **Figure 12**, the magnitude of CF_2 peak and CH_2 peak in neat-PTFE sample were decreased according to amination, furan modification and magnetite coupling. This is because the new appearance of other species like nitrogen or oxygen. By the same reason, the peak magnitude of Fluorine element was decreased by the modification. To be specific, for N_{1s} peak series, there was no peak in the neat-PTFE sample, but a new small peak was created after amination of PTFE membrane at about 400 eV. This indicates the successful amine modification on the surface of PTFE membrane. Similar tendency could be seen at O_{1s} peak series. A peak at 531.26 eV that indicates the increased amount of oxygen was grown according to amine modification, furan modification and magnetite coupling. Especially, this growth was drastically observed after

magnetite coupling because there are enormous amount of hydroxyl groups at MG@PEG-Mal. To summarize, the change of C_{1s}, N_{1s}, O_{1s} and F_{1s} peak indicates the successful modification of amine, furan and MG@PEG-Mal on the PTFE membrane.

The change of Fe_{2p} peak that indicates the presence of magnetite was described at **Figure 13**. Only pitching spectra that looks like a noise were observed in neat-PTFE, aminated PTFE and furan-modified PTFE membrane samples. However, there were two characteristic peak were observed at 710 eV and 722 eV that representing the iron species after MG@PEG-Mal coupling on the furan-modified PTFE. This is the clear evidence of successful coupling of magnetite. The relative amount change of each species for all the procedure was described at **Table 6**. As correlated with the spectra, the carbon and fluorine species were decreased according to the procedure. Similarly, nitrogen and oxygen species were increased at suitable step of modification. Finally, there were no iron species detected in neat, aminated, furan-modified PTFE, but 1.68% of iron species were observed after magnetite coupling. This result also supports the new appearance of iron peak described at Figure 13. To summarize the result, the successful modification with amine, furan and MG@PEG-Mal on the surface

of neat-PTFE membrane was clearly proved by XPS measurement.

The change of surface morphology due to the modification with several species was directly observed with FE-SEM observation. As seen at **Figure 14**, neat-PTFE membrane had the uneven shaped pores between PTFE polymers on the surface. After amination and furan-modification, this morphology was not changed. This indicates the UV treatment and chemical modification on the surface were not damaged the morphology of PTFE membrane. However, there was an obvious change after MG@PEG-Mal coupling on the furan-modified PTFE membrane. There were clusters that composed with magnetite nanoparticles were attached on the PTFE polymers between the pores. Some of the clusters were attached inside the pores, but the majority of magnetite appeared at the surface. Compared with furan-modified PTFE, this clusters newly appeared. Therefore, this indicates the successful modification of PTFE membrane with magnetite nanoparticles. EDS analysis supports this result. As described at **Figure 15**, a new peak that indicates the Fe species was created in MG-PTFE sample. This peak was not observed in furan-modified PTFE membrane. Also, the wide distribution of iron species could be directly observed by mapping result. To summarize the FE-SEM result, magnetite nanoparticle clusters were successfully attached

on the surface of PTFE membrane by Diels-Alder cycloaddition.

The change of hydrophilicity according to the modification of PTFE membrane with several species was defined by contact angle measurement. **Figure 16** describes the result. Neat-PTFE was highly hydrophobic because of hydrophobic nature of PTFE itself. The contact angle of DI water was 140.45° and this was the highest value between the samples. After amine modification, the contact angle of DI water was slightly decreased and becomes 134.79°. This is because amine functionalities on the surface of PTFE membrane was more hydrophilic than PTFE. The hydrogen bonding formed between nitrogen and hydrogen boosted the hydrophilic nature of amine functionalities. Same tendency was observed after furan modification, but the degree of decreased contact angle was more drastic and becomes 119.05°. This is because the nice hydrophilicity of Furfuryl glycidyl ether. Finally, the water contact angle was rapidly decreased to 90.19° after MG@PEG-Mal coupling. Clearly, the hydrophilicity of MG@PEG-Mal was the highest because of hydrophilic nature of PEG and hydroxyl group on the surface of magnetite nanoparticles. In conclusion, the hydrophilicity of hydrophobic PTFE membrane was varied due to amination, furan modification and MG@PEG-Mal coupling according to the contact angle

measurement.

Magnetic rotation-induced vortex on the surface of MG-PTFE membrane was directly observed by PIV observation. As described at **Figure 17**, PIV result was portrayed in flood form. Blue-colored region indicates the static region and red-colored region was relevant to turbulent flow that liquids are flow rapidly at a speed of maximum 0.2 mm/s. For neat-PTFE sample, there were only static region and just a slow-speed of flow on the surface. This result was observed in both presence and absence of magnetic rotation condition. This is because there was no force to drive the water at the surface of PTFE membrane. Magnetic rotation could not affect the water. In the case of MG-PTFE, however, there was a significant difference between no-rotation condition and magnetic rotation condition. Under the no-rotation condition, the PIV observation result was not so much different with static neat-PTFE result. After the magnetic-rotation was applied, the red-colored regions that indicate the turbulent flow of water were created in places of the PTFE membrane surface. Also, the average flow speed of membrane surface was increased to about 0.1 mm/s level. This is because the magnetite nanoparticles on the surface of MG-PTFE membrane were rotated due to the external magnetic-rotation and created the vortex of water. The

hydrophilic PEG-Mal polymer can easily drag the water so that enough amount of vortex was induced by the magneto-induced rotation on the membrane surface. This tendency was not only observed in the specific area of MG-PTFE membrane, but also appeared all over the MG-PTFE membrane surface. **Figure 18** supports this fact. To arrange the result generally, magnetite nanoparticles on the surface of MG-PTFE were created the magneto-induced vortex that could be observed by PIV observation.

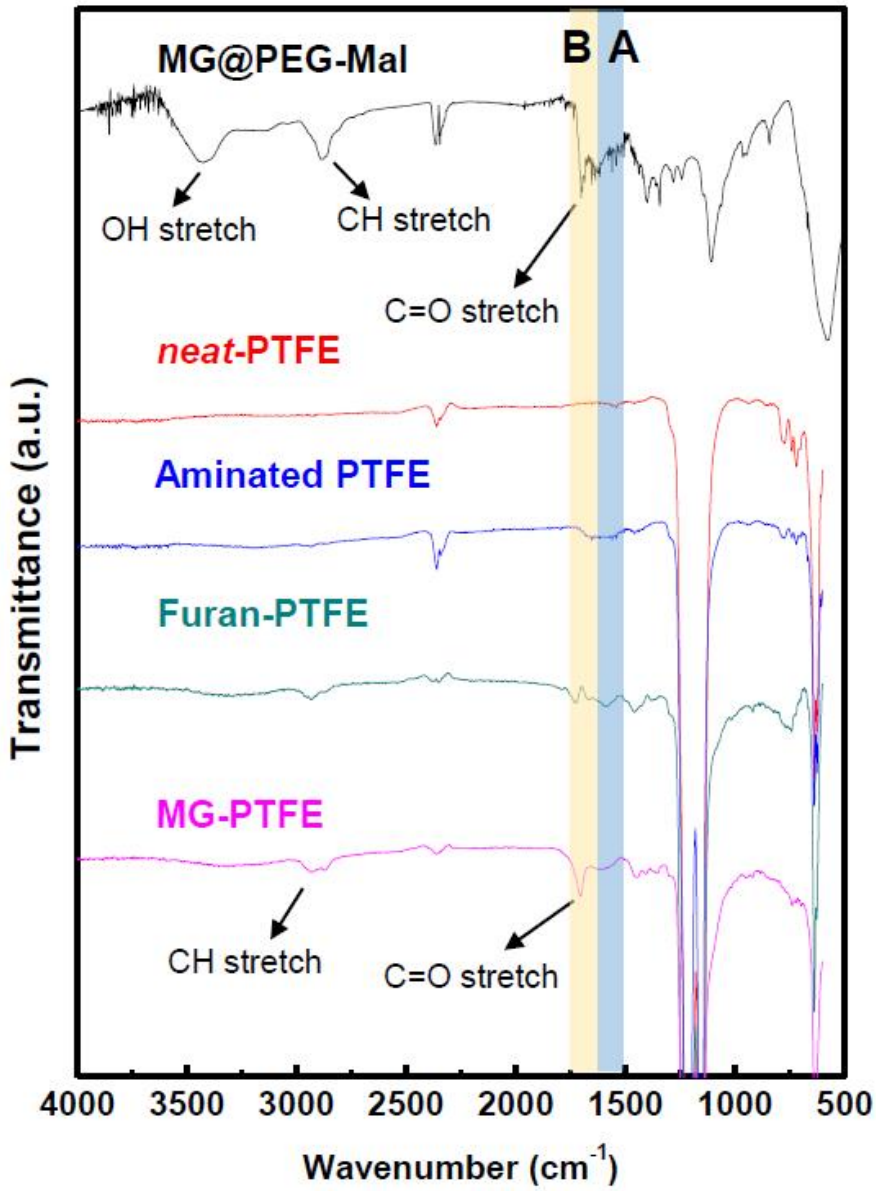

Figure 10. ATR FT-IR spectra of PTFE membranes

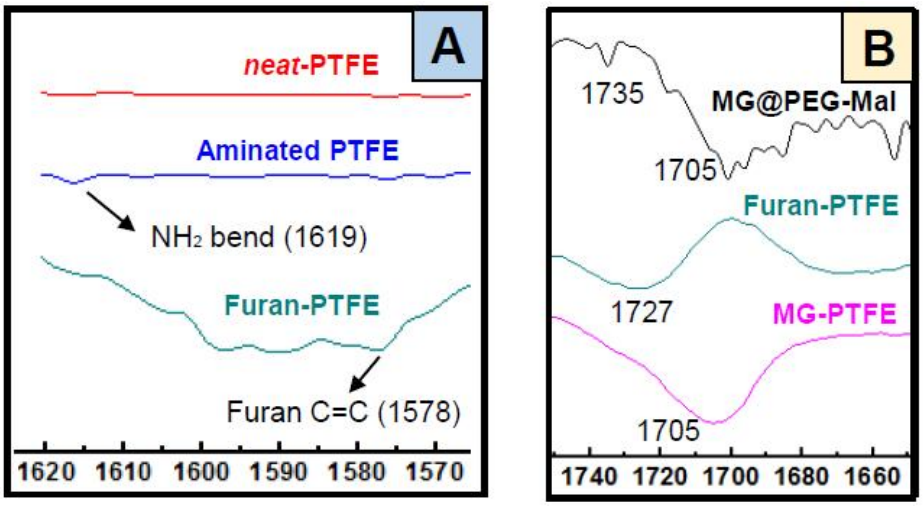

Figure 11. Magnified characteristic peaks of PTFE membrane samples

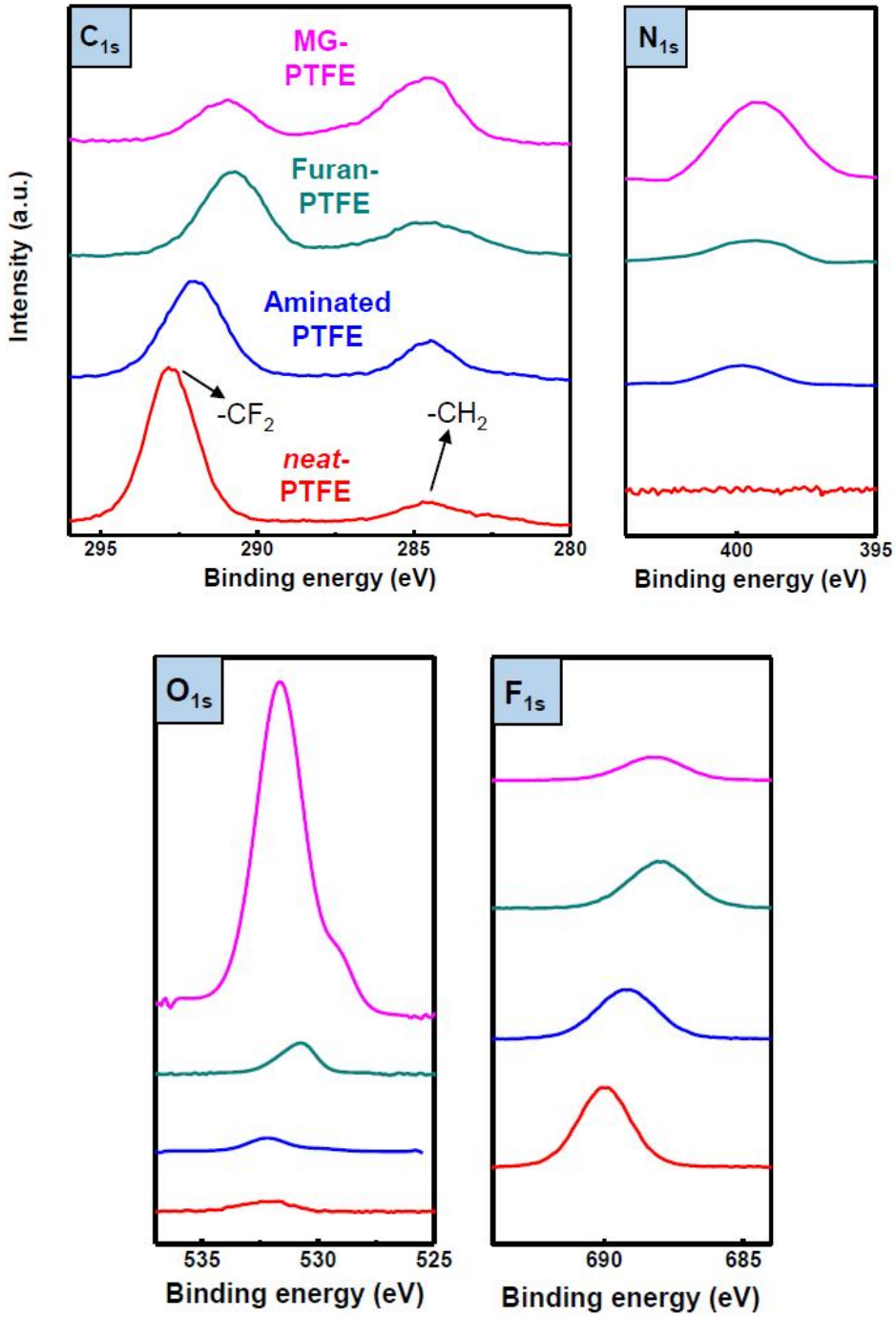

Figure 12. XPS spectra of membrane samples

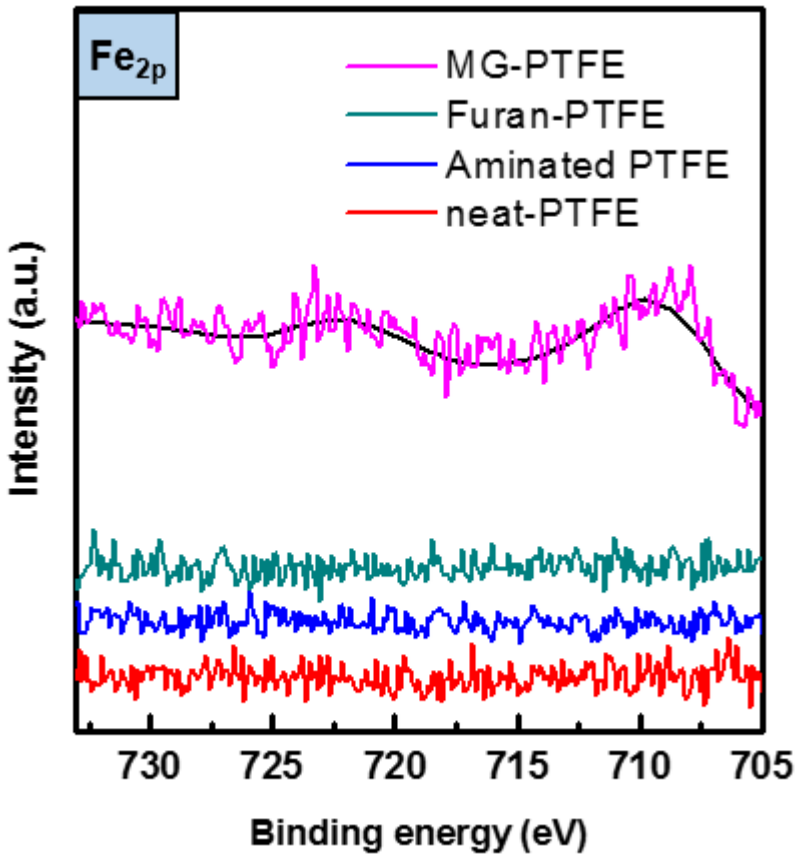

Figure 13. XPS spectra of membrane samples for iron species

	C (atomic conc. %)	N (atomic conc. %)	O (atomic conc. %)	F (atomic conc. %)	Fe (atomic conc. %)
neat-PTFE	32.33	-	0.68	66.99	-
Aminated PTFE	27.97	0.56	1.36	70.11	-
Furan-PTFE	33.30	0.69	2.76	63.25	-
MG-PTFE	47.54	1.63	11.84	37.31	1.68

Table 6. Quantitative inspection result of XPS measurement

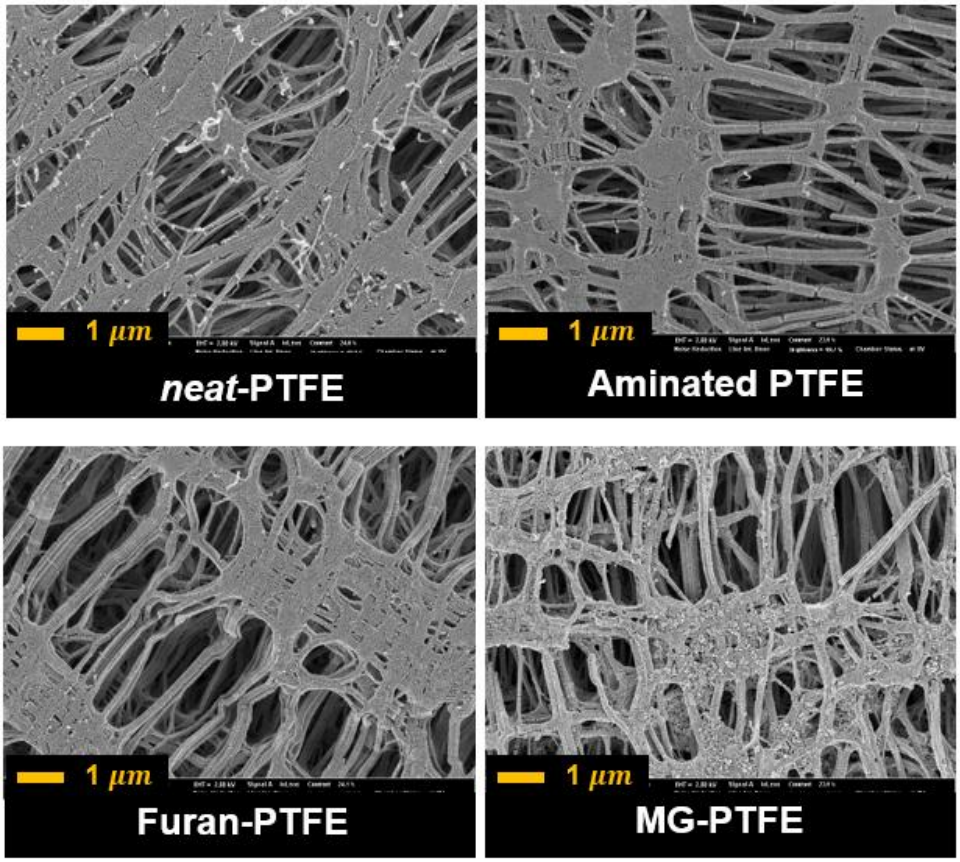

Figure 14. FE-SEM images of membrane samples

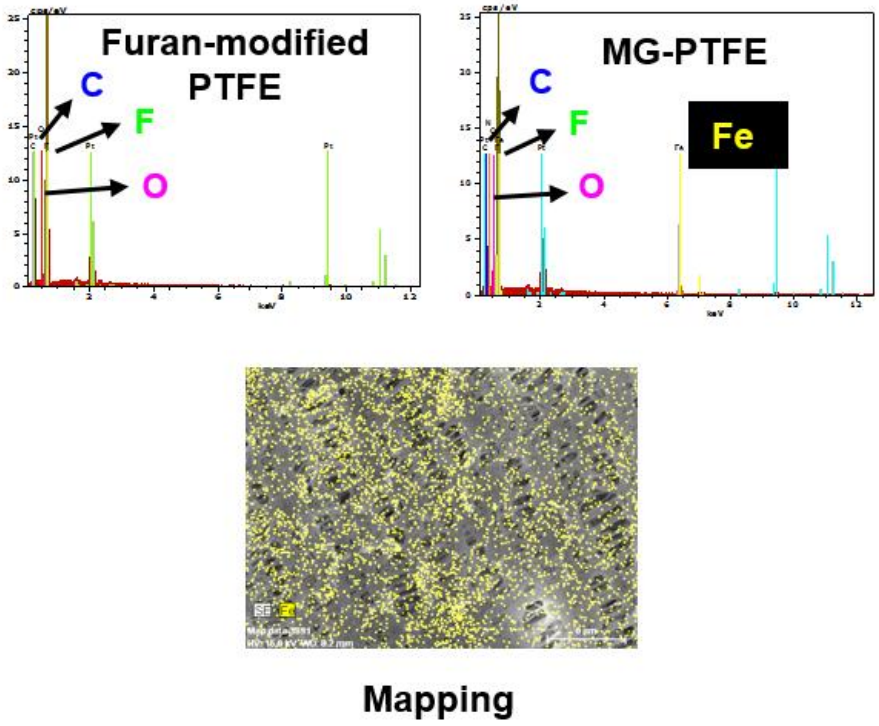

Figure 15. EDS analysis of furan-modified PTFE and MG-PTFE

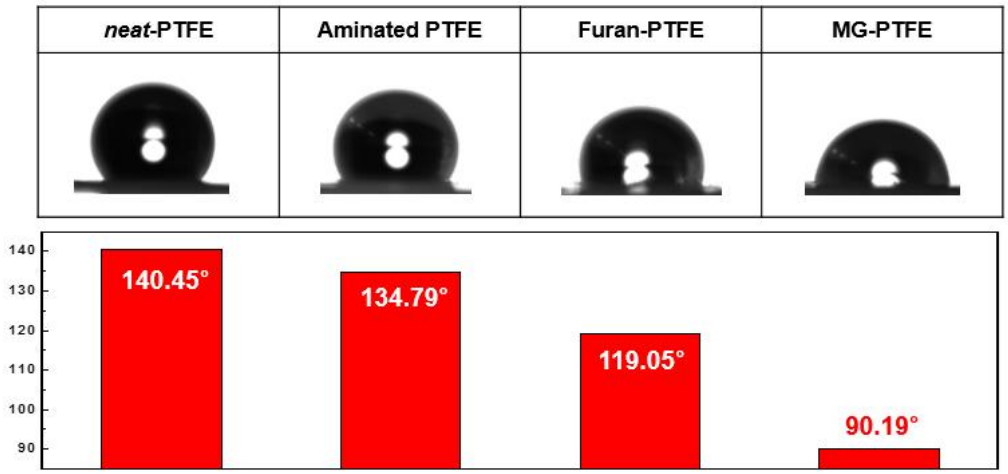

Figure 16. Varying contact angle of PTFE membrane samples

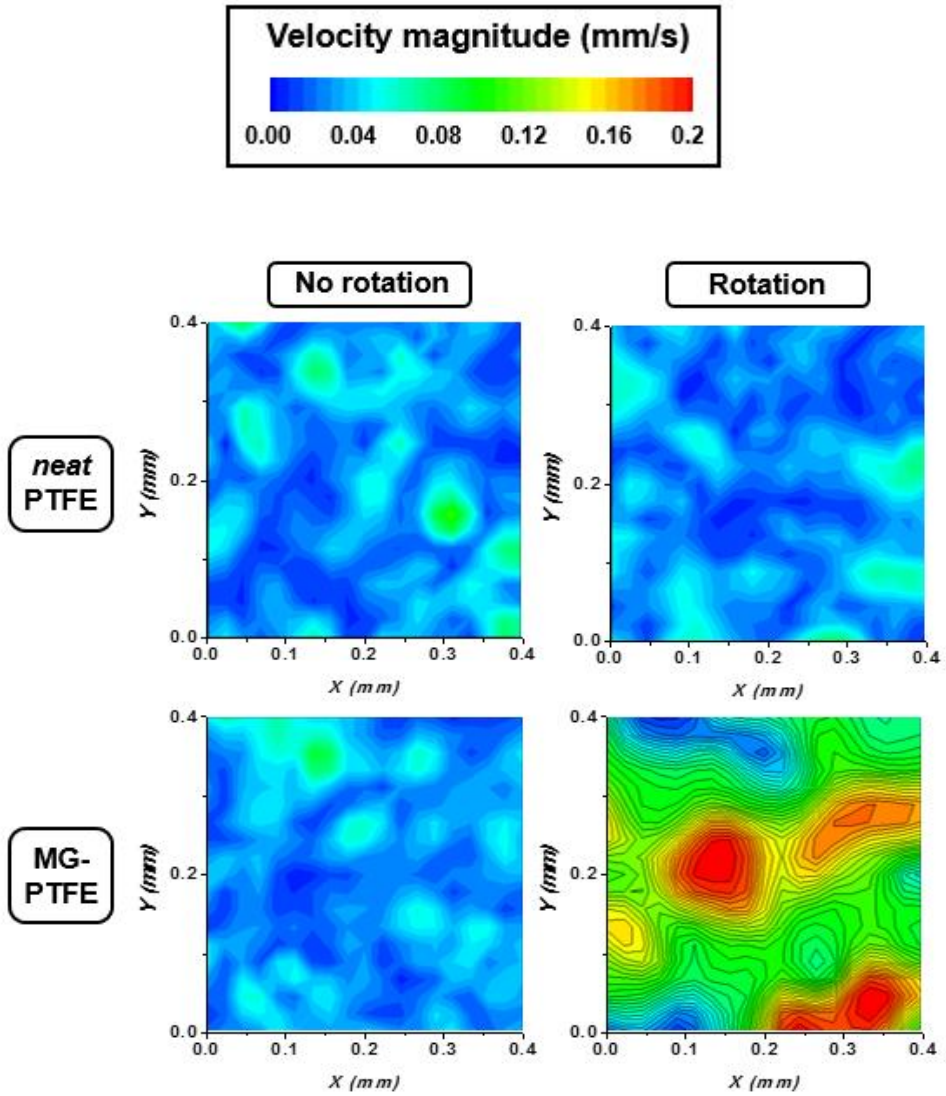

Figure 17. PIV observation of neat PTFE and MG-PTFE

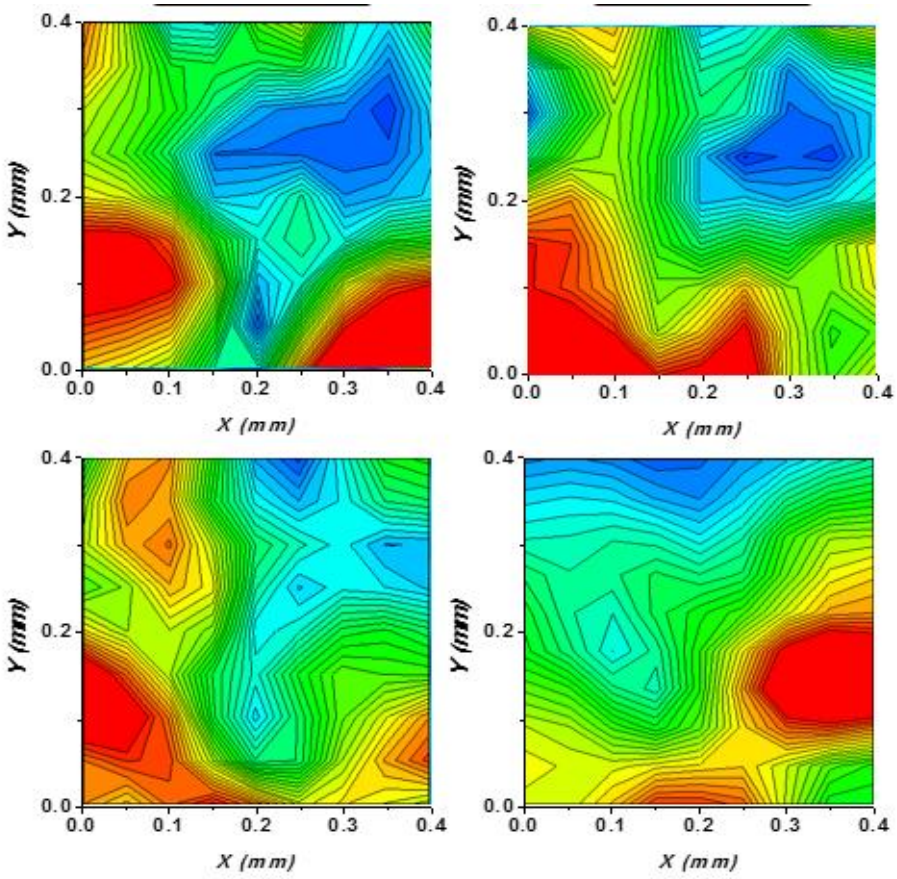

Figure 18. PIV observation in several area of MG-PTFE membrane

3.3. Reversible peel-and-stick process

Despite the fouling suppression effect of magneto-rotation induced vortex, irreversible fouling of PTFE membrane is inevitable. Irreversible fouling hinders the flow of water molecules so that water flux will be decreased. To avoid this fouling suppression effect, removal of irreversible fouling is necessary. Peel-and-stick process can replace fouled magnetite nanoparticles to new ones and easily restore water flux.

To evaluate the cleaning efficiency of MG-PTFE membrane, thermo-reversible peel-and stick process was operated. Heating was done by hot toluene with reflux and operating temperature of peel or stick process were 50 °C and 150 °C, respectively. Combination process of MG@PEG-Mal and furan-modified PTFE (stick process, Diels-Alder cycloaddition) was performed in hot oven and detachment of MG@PEG-Mal from furan-modified PTFE membrane (peel process, retro Diels-Alder cycloaddition) was done in hot oven with shaking to avoid aggregation of nanoparticles.

To evaluate the successful detachment and re-attachment of MG@PEG-Mal nanoparticles from the surface of furan-modified PTFE

membrane, ATR FT/IR spectra was used. The result was described in **Figure 19**. The most important characteristic peak of MG@PEG-Mal was C=O stretch in 1705 cm^{-1}, and this peak was vanished after retro Diels-Alder cycloaddition of MG@PEG-Mal nanoparticles. This is because the maleimide functionality of MG@PEG-Mal was removed from the PTFE membrane by peeling process. In other words, the removal of C=O stretch was a clear evidence for removal of MG@PEG-Mal nanoparticles. This removed C=O stretch re-appeared after attachment of MG@PEG-Mal nanoparticles again. Surely, the re-appearance of C=O peak indicated the re-attachment of MG@PEG-Mal nanoparticles. Also, as can be seen in **Figure 20**, C=C stretch for furan functionality of furan-modified PTFE membrane was observed at 1576 cm^{-1}. Therefore, the furan functionality was not affected by both Diels-Alder cycloaddition and retro Diels-Alder cycloaddition. To summarize, successful detachment and re-attachment of MG@PEG-Mal nanoparticles to the furan-modified PTFE membrane by rDA and DA reaction were determined using ATR FT-IR spectroscopy.

The change of membrane surface morphology according to thermal treatment was observed by FE-SEM. The result was portrayed in **Figure 21**. For MG-PTFE membrane sample, MG@PEG-Mal nanoparticles were

attached to the surface of PTFE membrane. This nanoparticles were vanished in rDA-PTFE sample, that is, the membrane with peeling process of MG@PEG-Mal nanoparticles were performed. Some traces of nanoparticles can be investigated in the rDA-PTFE sample, but almost all of the MG@PEG-Mal nanoparticles were removed by rDA reaction. Also, regeneration of MG@PEG-Mal could be observed in regenerated MG-PTFE sample.

Finally, contact angle measurement was performed to evaluate the change of membrane hydrophilicity according to the presence of MG@PEG-Mal nanoparticles. In **Figure 22**, this change was described. The water contact angle of MG-PTFE membrane was 90.19°, and this contact angle was increased to 120.77° after detachment of MG@PEG-Mal nanoparticles. This value was almost corresponded with the contact angle measurement of furan-modified PTFE in **Figure 16**. Also, the water contact angle was decreased again to 90.13° after re-attachment of MG@PEG-Mal was done. This angle was almost adjacent to that of MG-PTFE membrane. Furan-modified PTFE membrane was highly hydrophobic and MG@PEG-Mal nanoparticles were relatively hydrophilic due to the presence of hydroxyl groups and hydrophilic PEG chains. Therefore, the change of hydrophilicity by the DA

and rDA cycloaddition was the clear evidence of detachment and re-attachment of MG@PEG-Mal nanoparticles on the surface of furan-modified PTFE membrane.

To summarize the result, the maleimide functionality of MG@PEG-Mal nanoparticles and furan functionality of furan-modified PTFE membrane were combined and dissociated by thermo-responsive DA and rDA reaction.

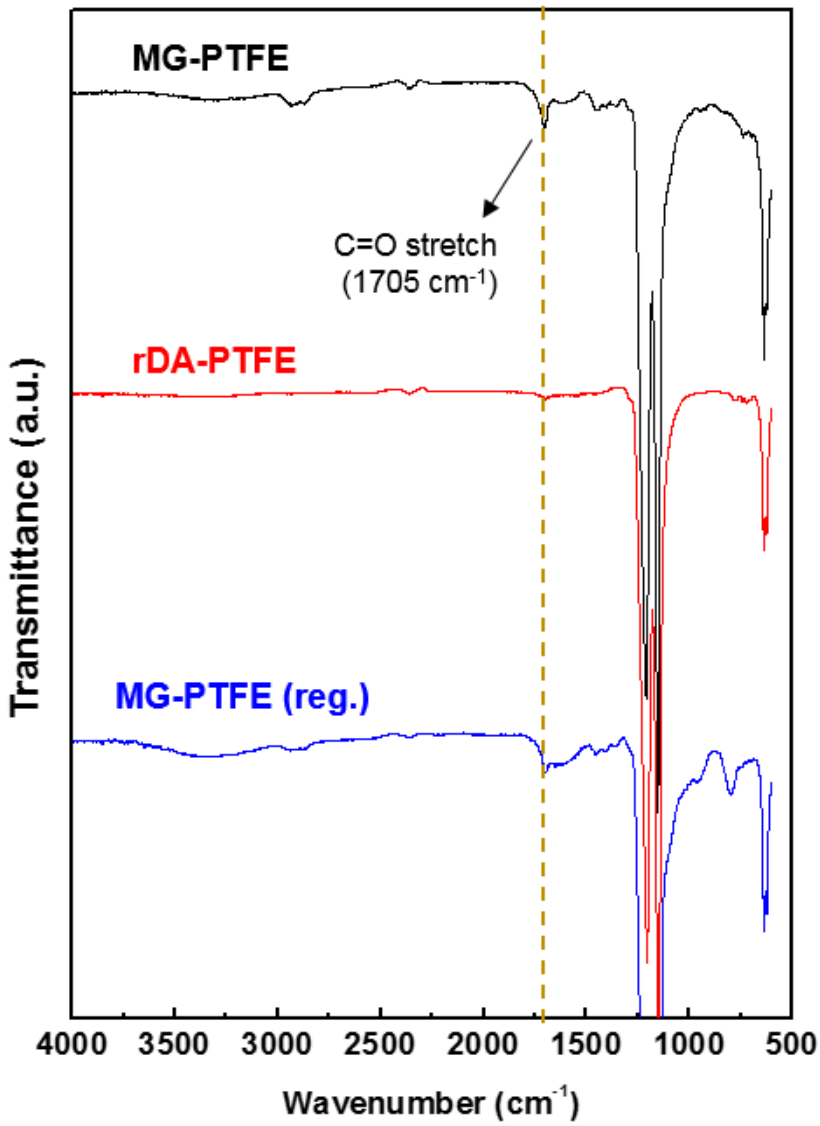

Figure 19. ATR FT-IR spectroscopy of PTFE membrane samples

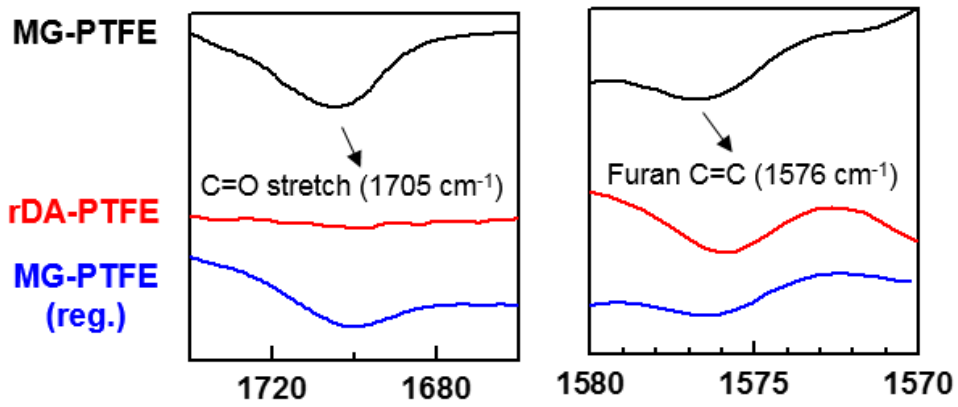

Figure 20. Change of characteristic peaks of PTFE membrane samples

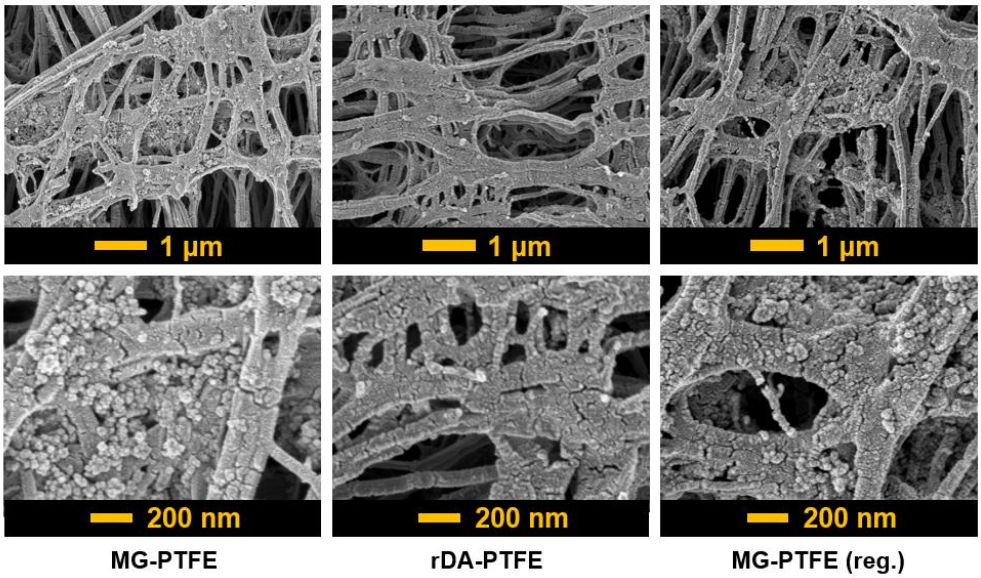

Figure 21. FE-SEM images of PTFE membrane samples

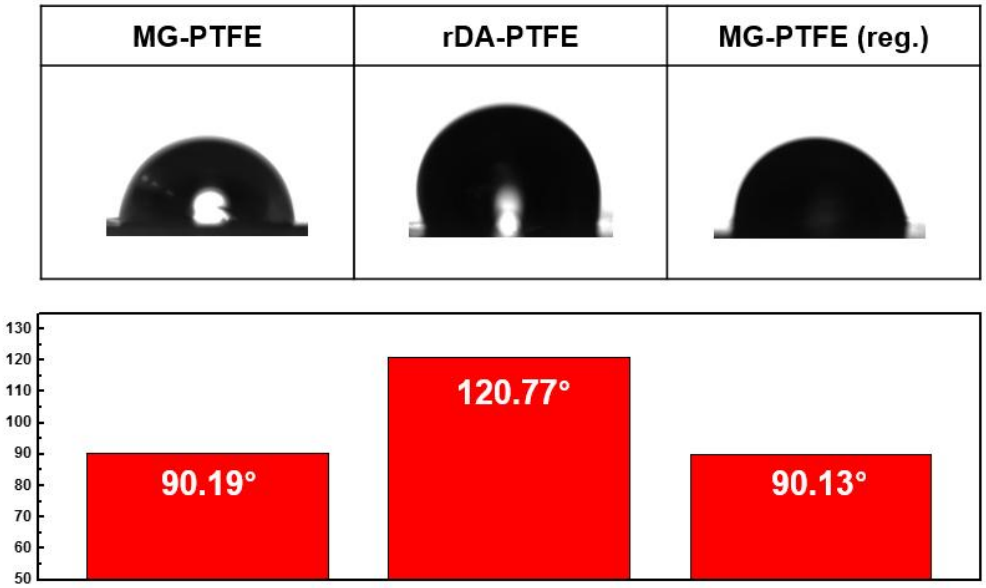

Figure 22. Contact angle measurement of PTFE membrane samples

3.4. Performance evaluation

3.4.1. Lysozyme filtration

Water filtration performance of MG-PTFE membrane was determined by filtration test using microfiltration cell system. Lysozyme, a typical organic foulant of UF membrane, was selected to evaluate anti-biofouling performance. The influence of magnetic rotation was observed by comparing static filtration system and magneto-rotating filtration system of MG-PTFE membrane. Finally, *neat*-PTFE membrane was used as a comparison group. The filtration result was described in **Figure 23**. First of all, the water flux of neat-PTFE membrane was dramatically decreased after insertion of 500 ppm Lysozyme solution. During 30 minutes of filtration with foulant solution, the water flux had decreasing tendency, consistently. Decreased water flux was recovered to 49% of initial flux after backwashing process. This is because the rejection of loosely attached foulants by water flux to opposite direction. This reduction and recovery of water flux was repeated for two times. Compared with neat-PTFE membrane, MG-PTFE

membrane had experienced less reduction of flux after insertion of foulant solution. Also, decreasing speed and degree of flux were both less than them of neat-PTFE membrane. After the backwashing process, the recovered flux of MG-PTFE membrane was 72% of initial flux. This value is 23% higher than that of *neat*-PTFE membrane. Similar tendency was observed in repeated process. This enhancement of anti-fouling property was amplified by magneto-induced rotation. For MG-PTFE membrane with magneto-induced rotation, recovered water flux was 81% of initial flux. In other words, MG-PTFE itself had some degree of anti-fouling effect, but MG-PTFE membrane with magneto-induced rotation was more effective anti-fouling behavior than MG-PTFE membrane without magneto-induced rotation. Therefore, MG@PEG-Mal modification and magneto-induced rotation were effective anti-fouling method for Lysozyme solution.

Quantitative analysis of fouling test result was described in **Figure 24.** Flux recovery ratio (FRR) was calculated for neat-PTFE, MG-PTFE without rotation and MG-PTFE with magneto-induced rotation sample. The calculation method of FRR was as follows:

$$\text{FRR} = \frac{J_R}{J_0} \times 100$$

Where J_R is the water flux of cleaned membrane and J_0 is the initial water flux. FRR of neat-PTFE membrane was 44.6%, but FRR was increased to 71.5% for MG-PTFE without magneto-rotation sample. This increase of FRR indicated the enhanced recovery of flux, that is, improved resistance to Lysozyme fouling. FRR of MG-PTFE with magneto-induced rotation sample was even more enhanced than MG-PTFE without magneto-induced rotation sample.

Also, the degree of membrane fouling was represented by calculated reversible and irreversible fouling resistance:

$$R_r = \frac{J_R - J_P}{J_0} \times 100$$

$$R_{ir} = \frac{J_0 - J_R}{J_0} \times 100$$

Where R_r and R_{ir} are the reversible and irreversible fouling resistance, respectively and J_p is the flux of foulant solution. R_r of neat-PTFE sample was poor as 19.7%, but that of MG-PTFE without magneto-induced rotation was much more enhanced to 34.4%. R_r of MG-PTFE with magneto-induced rotation was 32.5%. This enhancement of R_r indicated the increased anti-fouling property of MG-PTFE samples. Also, R_{ir} of neat-PTFE was

enormously high as 55.4%. However, R_{ir} of MG-PTFE without magneto-induced rotation was decreased to 28.5% and that of MG-PTFE with magneto-induced rotation was decreased again to 19.1%. This reduction of irreversible fouling indicated the well recovery of membrane filtration efficiency.

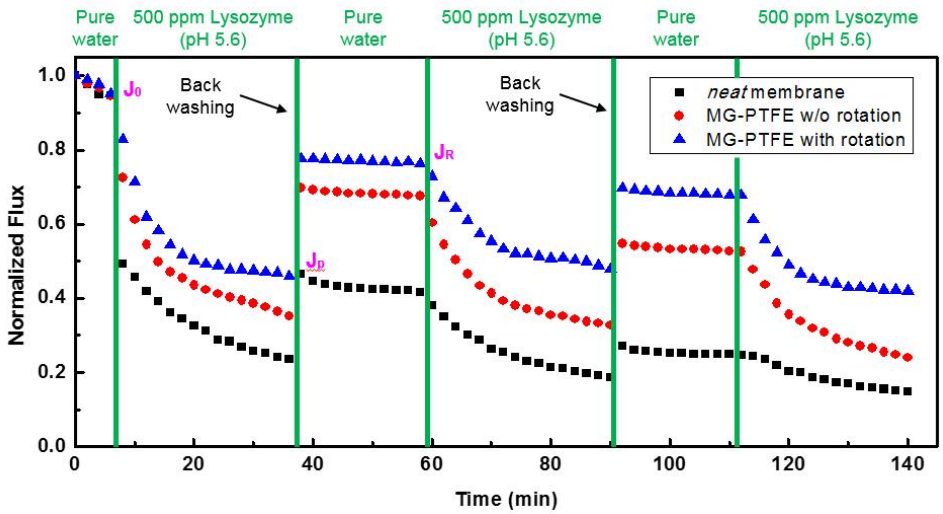

Figure 23. Membrane filtration test result with Lysozyme solution

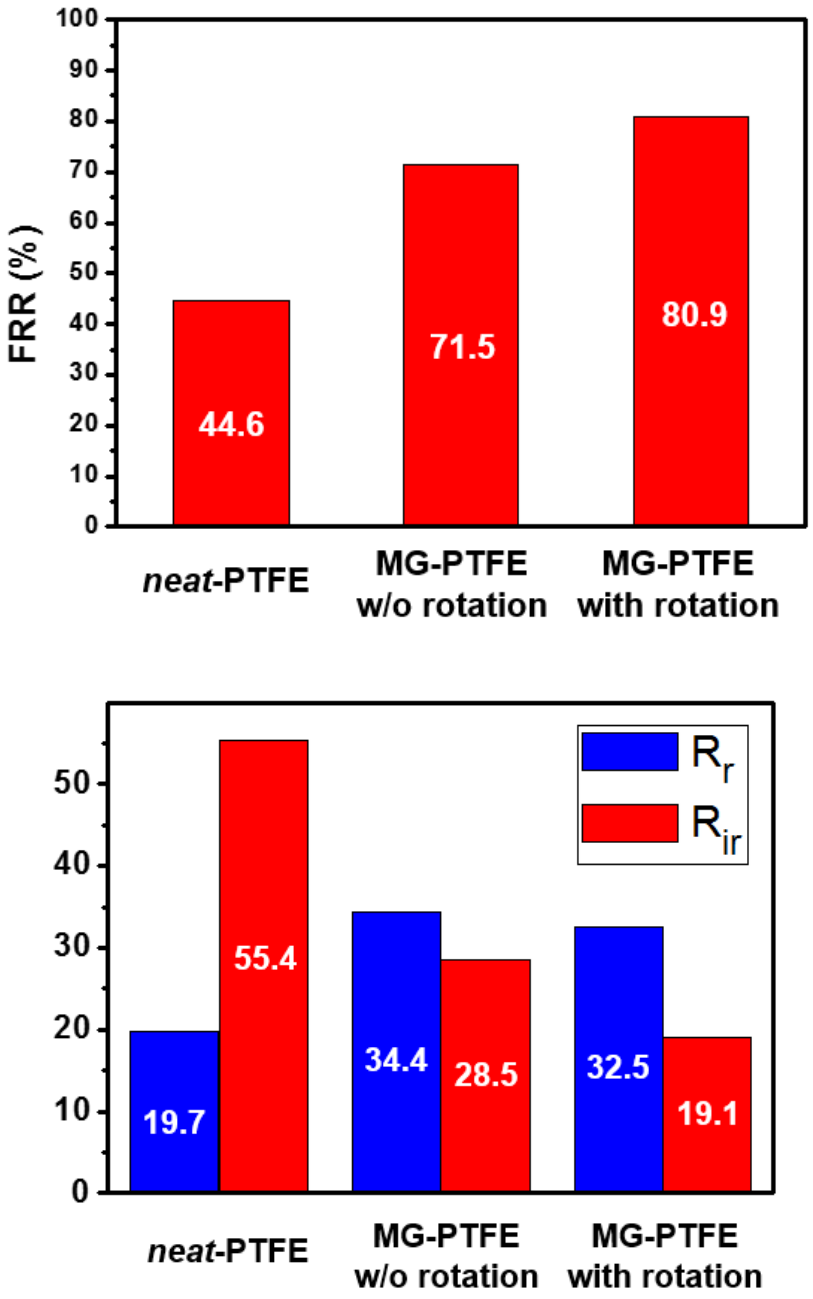

Figure 24. Quantitative analysis of Lysozyme filtration test result

3.4.2. Silica filtration

Similar anti-fouling efficiency test was performed for 500 ppm silica nanoparticle dispersion. As can be seen in **Figure 25**, the same tendency with Lysozyme filtration test case was observed. Water flux of neat-PTFE membrane was decreased drastically and hardly recovered to 45% of initial flux, but those of MG-PTFE with or without magneto-induced rotation were decreased slowly and recovered to 65% and 85% of initial flux, respectively. Therefore, MG@PEG-Mal modification and magneto-induced rotation were effective way of not only biofouling but anti-inorganic fouling.

The silica nanoparticle dispersion filtration result was analyzed quantitatively and described in **Figure 26.** FRR, R_r and R_{ir} were calculated using the same method with Lysozyme filtration result. FRR of neat-PTFE was 45.6%, but those of MG-PTFE without magneto-induced rotation and MG-PTFE with magneto-induced rotation were increased to 65.0% and 84.6%, respectively. This increased FRR means the enhanced anti-fouling property of MG-PTFE membrane. Next, R_r of all membranes samples were

not seriously changed, but R_{ir} value were dramatically decreased. R_{ir} of neat-PTFE membrane was 59.5%, but those of MG-PTFE without magneto-induced rotation and MG-PTFE with magneto-induced rotation were decreased to 38.1% and 20.4%, respectively. This enormous amount of R_{ir} reduction indicated the advanced anti-fouling property of MG-PTFE membrane samples. Also, the overall filtration efficiency of PTFE membrane was improved by MG@PEG-Mal modification and magneto-induced rotation.

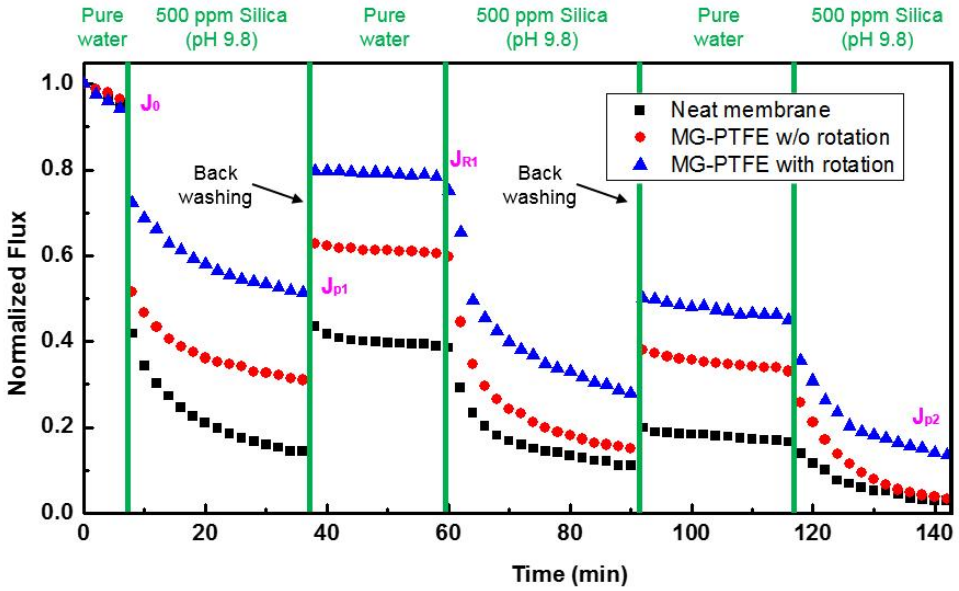

Figure 25. Membrane filtration test result with silica nanoparticle dispersion

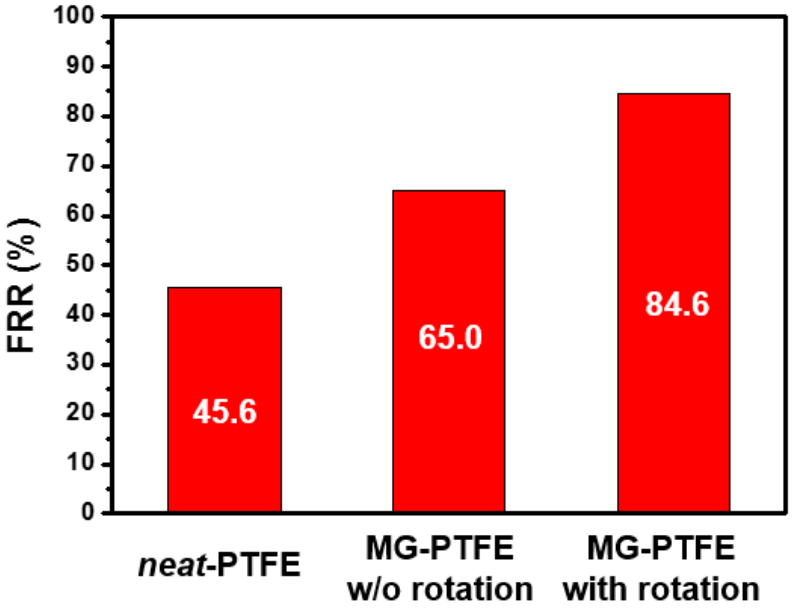
FRR (%)
100
90
80
70
60
50
40
30
20
10
0
45.6
65.0
84.6
neat-PTFE
MG-PTFE w/o rotation
MG-PTFE with rotation

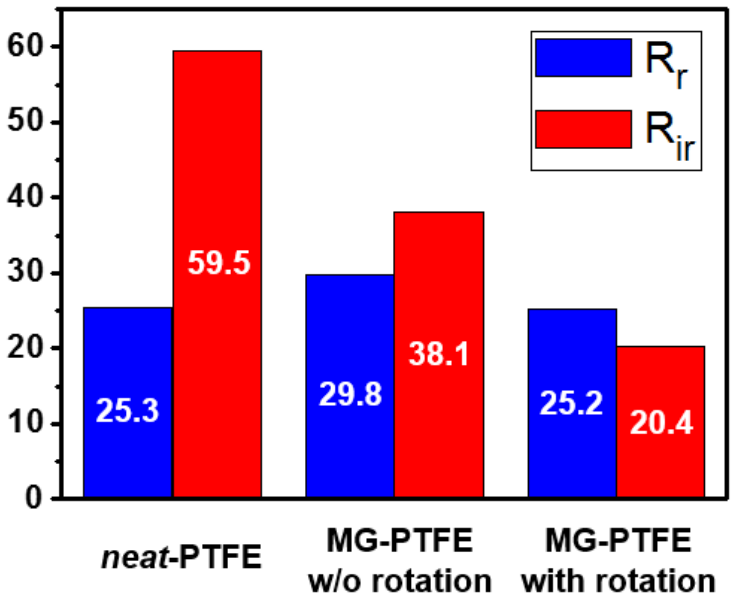
60
50
40
30
20
10
0
R_r
R_{ir}
25.3
59.5
29.8
38.1
25.2
20.4
neat-PTFE
MG-PTFE w/o rotation
MG-PTFE with rotation

Figure 26. Quantitative analysis of silica filtration test result

3.4.3. Comparison of cleaning efficiency

Cleaning efficiency of membranes samples after regeneration of MG@PEG-Mal were compared each other. Regeneration was done by retro Diels-Alder cycloaddition of contaminated MG@PEG-Mal nanoparticles and Diels-Alder cycloaddition of new MG@PEG-Mal nanoparticles. Even though there was no MG@PEG-Mal nanoparticles on neat-PTFE sample, the heating treatment at 50 ˚C and 150 ˚C was performed. The result was described in **Figure 27.** After the heating treatment, the water flux of neat-PTFE membrane was recovered, but the magnitude of recovered flux was relatively small. On the other hand, the water flux of MG-PTFE samples were recovered dramatically. The recovered water flux was almost similar with initial water flux. Therefore, regeneration of MG@PEG-Mal nanoparticles was effective way of recovering the decreased water flux.

The above result was quantitatively analyzed and described in **Figure 28.** FRR of neat-PTFE membrane was relatively low as 41.3%,

whereas those of MG-PTFE membrane without and with magneto-induced rotation were 74.9% and 79.7%, respectively. This high recovery of flux indicated the effective cleaning of contaminated membrane by regeneration of MG@PEG-Mal nanoparticles. The change of R_r and R_{ir} were also remarkable. R_r of neat-PTFE membrane was 38.3, but those of MG-PTFE membrane without and with magneto-induced rotation were 71.5 and 65.2, respectively. Compared with cleaning efficiency of backwashing process, R_r was greatly increased by regeneration of MG@PEG-Mal nanoparticles because the decreased water flux was recovered drastically. Finally, R_{ir} of the membrane samples were 58.7, 25.1 and 20.3, respectively. To summarize regeneration of MG@PEG-Mal nanoparticles were effective for flux recovery of fouled membrane.

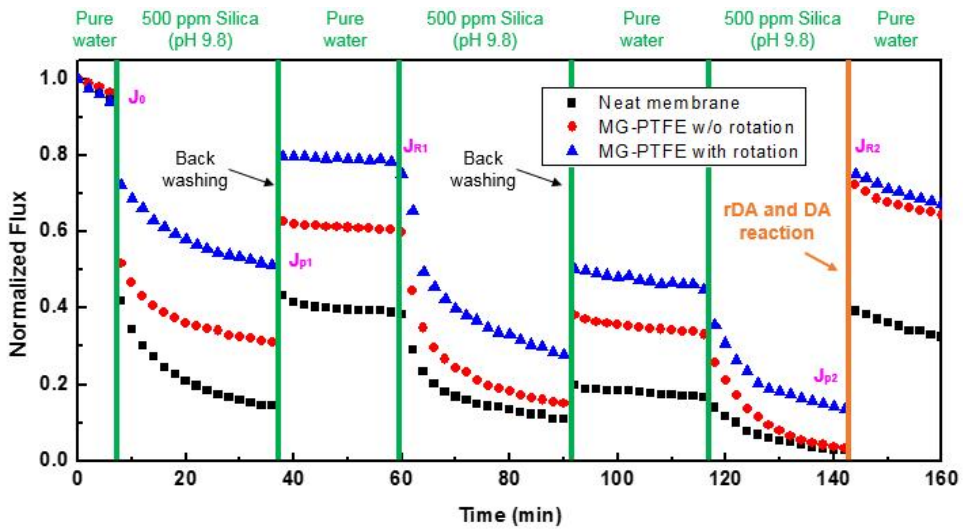

Figure 27. Comparison of cleaning efficiency by regeneration of MG@PEG-Mal

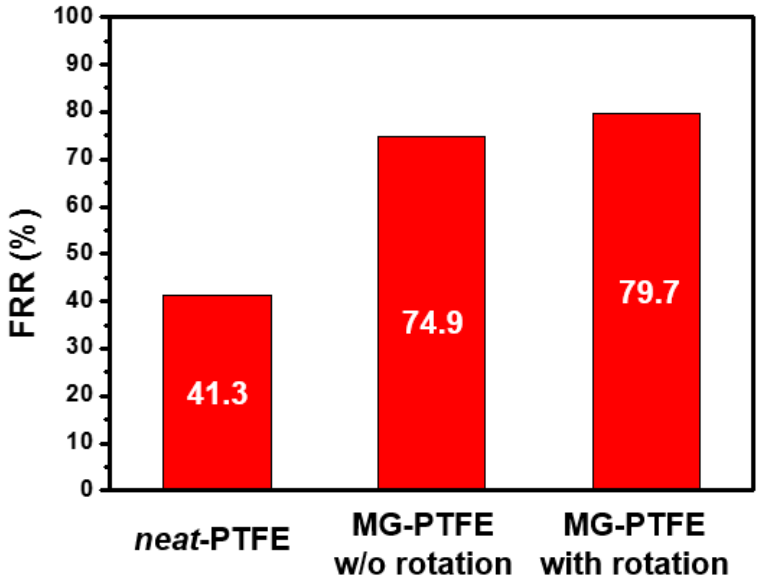
FRR (%)
100
90
80
70
60
50
40
30
20
10
0
41.3
74.9
79.7
neat-PTFE
MG-PTFE
w/o rotation
MG-PTFE
with rotation

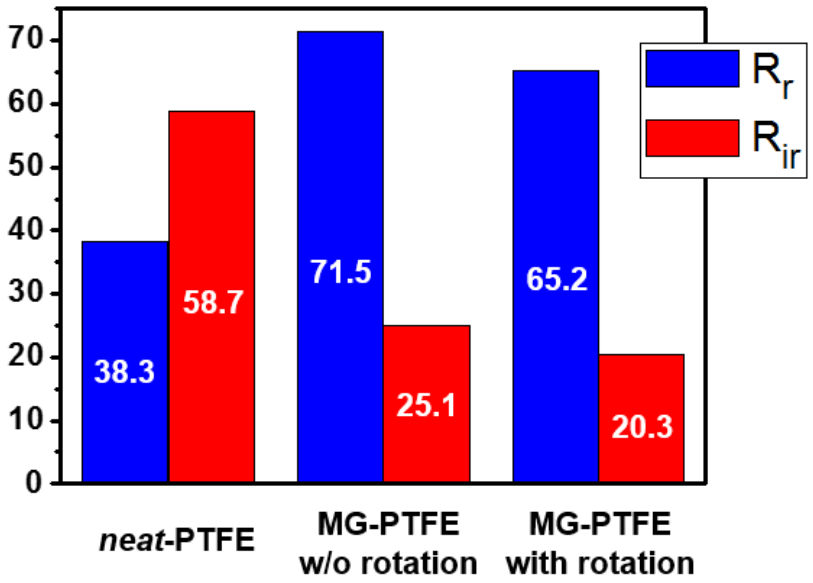

Figure 28. Quantitative analysis of cleaning efficiency test result

4. Conclusion

In this research, neat-PTFE membrane was modified with maleimide-terminated magnetite nanoparticles to observe the influence of magnetite nanoparticles on the fouling suppression efficiency of MF membrane system. Magnetite nanoparticles were synthesized by co-precipitation method with PEG-Mal polymer and two kinds of iron

precursors. The amount of PEG-Mal polymer was set as variables to find out the optimized amount for synthesizing MG@PEG-Mal and 1 g was defined as an optimized value. Synthesized MG@PEG-Mal sample was analyzed by various characterization method like FT-IR, XRD, TGA and VSM. Synthesized MG@PEG-Mal nanoparticles were attached to furan-modified PTFE membrane by thermo-responsive Diels-Alder cycloaddition. Fabricated MG-PTFE membrane was characterized by ATR FT-IR, XPS, FE-SEM, contact angle measurement and PIV observation. Successful fabrication of MG-PTFE membrane and effective movement of magnetite nanoparticles by external rotating magnetic field was observed. Water filtration test was operated to measure the anti-biofouling and anti-inorganic fouling property of MG-PTFE membrane by Lysozyme solution and silica nanoparticle dispersion. As a result, anti-fouling property of MG-PTFE membrane was enhanced about 20% without magneto-induced rotation, but anti-fouling property was advanced about 10% more with applied external rotating magnetic field. Finally, replacement of contaminated MG@PEG-Mal nanoparticles to new one was performed to measure the cleaning efficiency of MG-PTFE membrane by regeneration of MG@PEG-Mal nanoparticles. The decreased water flux was dramatically recovered to 80% of initial flux after regeneration of MG@PEG-Mal so that the peel-and-stick

process was effective way of membrane flux recovery. To summarize, MG-PTFE membrane had enhanced fouling resistance and cleaning efficiency compared with neat-PTFE membrane.

Fouling suppression is one of the most important issue in membrane filtration technology. Magneto-induced vortex can be a facile solution of fouling issue and renewability gives magneto-responsive anti-fouling membrane the economic and environmental efficiency. This combination of fouling suppression method and cleaning technique can be a next-generation smart cleaning method of membrane and applied in low-pressure operating condition such as submerged membrane system.

5. References

[1] Shannon, Mark A., et al. "Science and technology for water purification in the coming decades." *Nature* 452.7185 (2008): 301-310.

[2] Spiegler, Kurt Samuel, ed. *Principles of desalination*. Elsevier,

2012.

[3] Glaze, William H., Joon-Wun Kang, and Douglas H. Chapin. "The chemistry of water treatment processes involving ozone, hydrogen peroxide and ultraviolet radiation." (1987): 335-352.

[4] Jiuhui, Q. U. "Research progress of novel adsorption processes in water purification: A review." *Journal of Environmental Sciences* 20.1 (2008): 1-13.

[5] Van der Bruggen, Bart, et al. "A review of pressure-driven membrane processes in wastewater treatment and drinking water production." *Environmental progress* 22.1 (2003): 46-56.

[6] Field, R. W., et al. "Critical flux concept for microfiltration fouling." *Journal of Membrane Science* 100.3 (1995): 259-272.

[7] Maximous, Nermen, G. Nakhla, and W. Wan. "Comparative assessment of hydrophobic and hydrophilic membrane fouling in wastewater applications." *Journal of membrane Science* 339.1 (2009): 93-99.

[8] Kim, Dooil, et al. "Biocide application for controlling biofouling of SWRO membranes—an overview." *Desalination* 238.1 (2009): 43-52.

[9] Park, Sung Yong, et al. "Amphiphilic thiol functional linker mediated sustainable anti-biofouling ultrafiltration nanocomposite comprising a silver nanoparticles and poly (vinylidene fluoride) membrane." *ACS applied materials & interfaces* 5.21 (2013): 10705-10714.

[10] Perreault, Francois, Marissa E. Tousley, and Menachem Elimelech. "Thin-film composite polyamide membranes functionalized with biocidal graphene oxide nanosheets." *Environmental Science & Technology Letters* 1.1 (2013): 71-76.

[11] Albu, Sergiu P., et al. "Self-organized, free-standing TiO2 nanotube membrane for flow-through photocatalytic applications." *Nano letters* 7.5 (2007): 1286-1289.

[12] Tokarev, Ihor, et al. "Stimuli-responsive hydrogel membranes coupled with biocatalytic processes." *ACS applied materials & interfaces* 1.3 (2009): 532-536.

[13] Ying, Jackie Y., and Cindy Ren. "Thermo-responsive materials." U.S. Patent Application No. 12/279,461.

[14] Valeur, Bernard, and Isabelle Leray. "Ion-responsive supramolecular fluorescent systems based on multichromophoric calixarenes:

a review." *Inorganica chimica acta* 360.3 (2007): 765-774.

[15] Reinicke, Stefan, et al. "Magneto-responsive hydrogels based on maghemite/triblock terpolymer hybrid micelles." *Soft Matter* 6.12 (2010): 2760-2773.

[16] Lynn, David M., Mansoor M. Amiji, and Robert Langer. "pH-responsive polymer microspheres: Rapid release of encapsulated material within the range of intracellular pH." *Angewandte Chemie International Edition* 40.9 (2001): 1707-1710.

[17] Qiu, Yong, and Kinam Park. "Environment-sensitive hydrogels for drug delivery." *Advanced drug delivery reviews* 53.3 (2001): 321-339.

[18] Zhang, Qiaolan, et al. "Wettability switching between high hydrophilicity at low pH and high hydrophobicity at high pH on surface based on pH-responsive polymer." *Chemical Communications* 10 (2008): 1199-1201.

[19] Varley, Russell John, and Sybrand van der Zwaag. "Autonomous damage initiated healing in a thermo-responsive ionomer." *Polymer International* 59.8 (2010): 1031-1038.

[20] Zhang, Yunfei, et al. "DNA-capped mesoporous silica nanoparticles as an ion-responsive release system to determine the presence of mercury in aqueous solutions." *Analytical chemistry* 84.4 (2012): 1956-1962.

[21] Sumalekshmy, S., and Christoph J. Fahrni. "Metal-Ion-Responsive Fluorescent Probes for Two-Photon Excitation Microscopy†." *Chemistry of Materials* 23.3 (2010): 483-500.

[22] Zeng, Jing, et al. "Biodegradable electrospun fibers for drug delivery." *Journal of Controlled Release* 92.3 (2003): 227-231.

[23] Ren, Liang, et al. "Design and application of a fiber Bragg grating strain sensor with enhanced sensitivity in the small-scale dam model." *Smart Materials and Structures* 18.3 (2009): 035015.

[24] Schmaljohann, Dirk. "Thermo-and pH-responsive polymers in drug delivery." *Advanced drug delivery reviews* 58.15 (2006): 1655-1670.

[25] Lentacker, Ine, et al. "Ultrasound-responsive polymer-coated microbubbles that bind and protect DNA." *Langmuir* 22.17 (2006): 7273-7278.

[26] Chu, Liang-Yin, et al. "Preparation of thermo-responsive core-shell

microcapsules with a porous membrane and poly (N-isopropylacrylamide) gates." *Journal of Membrane Science* 192.1 (2001): 27-39.

[27] Park, Sung Yong, Jae Woo Chung, and Seung-Yeop Kwak. "Regenerable anti-fouling active PTFE membrane with thermo-reversible “peel-and-stick” hydrophilic layer." *Journal of Membrane Science* 491 (2015): 1-9.

[28] Meng, Jianqiang, et al. "A novel salt-responsive TFC RO membrane having superior antifouling and easy-cleaning properties." *Journal of Membrane Science* 461 (2014): 123-129.

[29] Thévenot, Julie, et al. "Magnetic responsive polymer composite materials." *Chemical Society Reviews* 42.17 (2013): 7099-7116.

[30] Yu, Xi, et al. "Reversible pH-Responsive Surface: From Superhydrophobicity to Superhydrophilicity." *Advanced Materials* 17.10 (2005): 1289-1293.

[31] Wandera, Daniel, S. Ranil Wickramasinghe, and Scott M. Husson. "Stimuli-responsive membranes." *Journal of Membrane Science* 357.1 (2010): 6-35.

[32] Wee, Kin-Ho, and Renbi Bai. "Stimuli-Responsive Membranes." *Encyclopedia of Membrane Science and Technology* (2013).

[33] Yu, Sanchuan, et al. "Intensified cleaning of organic-fouled reverse osmosis membranes by thermo-responsive polymer (TRP)." *Journal of membrane science* 392 (2012): 181-191.

[34] Meng, Jianqiang, et al. "A novel salt-responsive TFC RO membrane having superior antifouling and easy-cleaning properties." *Journal of Membrane Science* 461 (2014): 123-129.

[35] Himstedt, Heath H., et al. "Magnetically activated micromixers for separation membranes." *Langmuir* 27.9 (2011): 5574-5581.

[36] Gribble, Gordon W. "Diels–Alder Cycloaddition." *Indole Ring Synthesis: From Natural Products to Drug Discovery*: 437-463.

국문초록

본 연구에서는 자성나노입자를 열 감응성 동적공유결합을 이용해 폴리테트라플루오로에틸렌(PTFE) 정밀여과 분리막 표면에 결합하여 열과 자성의 두 가지 자극에 동시에 감응하는 분

리막을 제조하였다. 이 분리막은 자성입자의 회전이 발생시킨 와류로 인해 우수한 내파울링성능과 향상된 세척효율을 보였다. 제조과정에서 온도의 변화에 감응하여 결합을 형성 혹은 해리시킬 수 있는 퓨란과 말레이미드의 딜스-알더 고리화첨가반응이 이용되었다. 표면에 말레이미드기가 부착된 자성입자를 두 종류의 철 전구체와 말레이미드로 개질된 폴리에틸렌글리콜 고분자의 공침반응을 통해 합성하였다. 기공크기 0.1 μm의 PTFE 분리막은 UV조사를 통해 표면에 퓨란기를 부여한 후 말레이미드로 개질된 자성입자를 결합하여 자성입자가 부착된 PTFE 분리막을 제조하였다. 이상의 과정에서 FT-IR, XRD, TGA, VSM, XPS, FE-SEM, 접촉각측정법 등을 이용하여 분리막과 자성입자의 특성을 평가하였다. 특히, 자성입자가 외부 자기장의 회전에 감응하여 실제로 와류를 발생시키는가에 대한 확인은 PIV분석을 통해 이루어졌다. 이러한 분리막의 내파울링 성능을 라이소자임과 실리카 나노입자의 두 가지 종류의 파울런트를 이용하여 평가한 결과 자성입자로 개질된 분리막은 일반 분리막에 비해 파울런트에 의한 수투과도의 감소폭이 적었다. 또한 역세공정을 통한 수투과도의 복원율 역시 일반 분리막과 비교했을 때 자성입자 개질을 통해 44.6% 에서 80.9% 로 크게 향상되었다. 오염된 분리막 표면은 자성나노입자의 재생을 통해 복구될 수 있으며 이는 막오염에 따라 감소했던 수투과도가 자성나노입자의 재생 후 초기

수투과도의 80% 수준으로 매우 높게 복원되는 것을 통해 확인할 수 있었다. 이러한 자성-감응성 내파울링 효과와 재생가능성 분리막의 결합을 통해 분리막의 내파울링성을 향상시키는 데 있어 시너지 효과를 유발할 수 있었다. 이러한 분리막은 침지식 분리막 공정과 같이 파울런트의 종류가 복합적이고 농도가 비교적 높은 공정에서 응용될 수 있을 것으로 기대된다.